proliferation were comparable between control and silenced cells (Fig. 1d); however, miR122-silenced cells exhibited a larger number of distinct pseudopodia (Fig. 1e). Next, as miR122 is specifically expressed in the liver, we hypothesized that it may have a role in hepatocyte differentiation and, therefore, we investigated the expression of several hepatocyte markers by semi-quantitative RT–PCR. We observed an increase in AFP expression and a slight elevation of albumin expression in miR122-silenced cells, but the expression levels of other hepatocyte markers, such as hepatocyte nuclear factor 4α (HNF4α) and α_1-antitrypsin, did not change (Fig. 1f).

MiR122-silenced HCC cells exhibit a more invasive phenotype. Because miR122-silenced cells exhibited an increased number of pseudopodia, we next characterized phenotypes associated with more biologically aggressive cell characteristics. We found that actin polymerization and pseudopod formation were significantly increased in miR122-silenced cells (Fig. 2a). The increase in the number of pseudopodia was confirmed by a quantitative pseudopodia assay (Supplementary Fig. S1). Although the expression levels of the mesenchymal marker α-smooth muscle actin were only slightly increased, we observed a significant decrease in the expression of the epithelial marker E-cadherin in miR122-silenced cells (Fig. 2b). Furthermore, the expression of other epithelial-to-mesenchymal transition markers such as fibronectin, N-cadherin, snail and Zeb1 was altered in miR122-silenced cells (Supplementary Fig. S1). These findings are consistent with the notion that loss of miR122 function leads to a more malignant phenotype.

We next performed scratch and invasion assays to characterize the invasive phenotype of miR122-silenced cells. Rates of cell migration and of cell invasion were significantly increased in miR122-silenced cells (Fig. 2c,d). As the proliferation rates of control and miR122-silenced cells were similar (Fig. 1d), altogether these results suggest that inhibition of miR122 function in HCC cells may lead to increases in malignancy-related cellular properties.

To investigate the molecular mechanisms underlying these cellular phenotypes, we assessed the activity of RhoA and Rac1, which are small GTPases that are closely associated with cell migration and invasion[28]. Although Rac1 activity did not significantly change, RhoA activity significantly increased in miR122-silenced cells (Fig. 2e), suggesting that the increase in cell migration and invasion in miR122-silenced cells may result from increased RhoA activity.

AFP expression is increased in miR122-silenced HCC cells. As we observed an increase in AFP expression in miR122-silenced cells (Fig. 1f), we next sought to quantify AFP concentrations in culture supernatants using an enzyme-linked immunosorbent assay (ELISA). AFP levels were approximately three times higher in the supernatant of miR122-silenced cells as compared with control cells (Fig. 3a). Consistent with this observation, immunofluorescence staining for AFP produced a stronger cytoplasmic signal and quantitative RT–PCR revealed a tenfold increase in AFP mRNA levels in miR122-silenced cells (Fig. 3b,c).

The 3′-UTR of the AFP mRNA did not contain predicted miR122 target sequences, based on sequence analyses performed using miRNA target search engines such as TargetScan (http://www.targetscan.org), suggesting that it is unlikely that miR122 directly regulates AFP expression. Therefore, to characterize the mechanisms underlying increased AFP expression in miR122-silenced cells, we first assessed the stability of the AFP mRNA in miR122-silenced cells. As expected, AFP mRNA stability was unaffected by silencing of miR122, as the amount of mRNA was comparable between control and miR122-silenced cells at 6, 12 and 24 h after inhibition of new transcription by treatment with actinomycin D (Fig. 3d). The increase in AFP mRNA levels in the absence of changes in mRNA stability suggested that transcription of AFP was increased

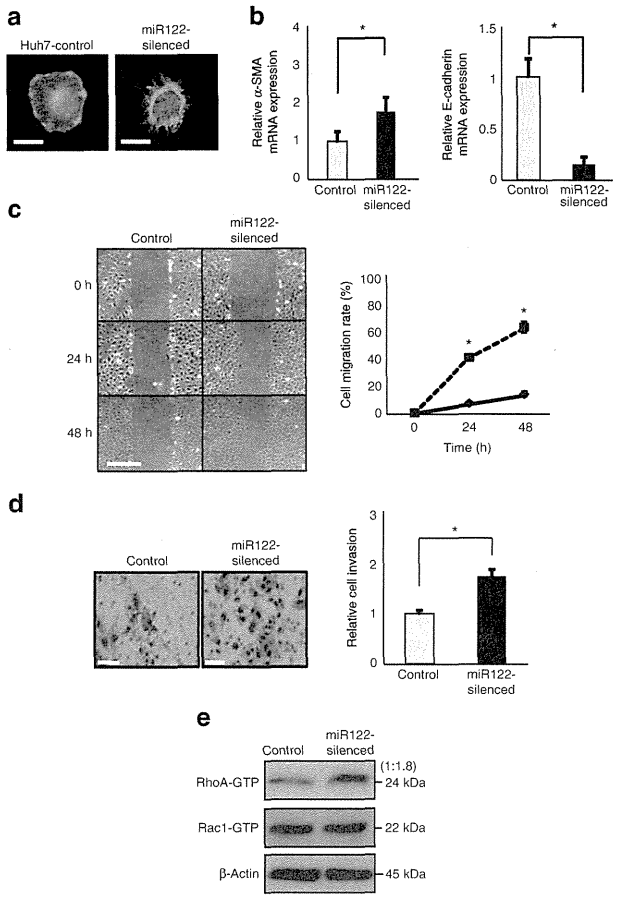

Figure 2 | HCC cells silenced for miR122 function exhibit a more invasive phenotype. (**a**) Cells were treated with 2 ng ml^{-1} TGF-β for 12 h, and actin filaments were stained with Alexa Fluor 488-conjugated phalloidin. Representative results from two independent experiments using Huh7 cells are shown. Similar results were obtained using PLC/PRF/5 cells. Scale bar, 50 μm. (**b**) Expression levels of α−smooth muscle actin and E-cadherin mRNAs were assessed by quantitative RT–PCR. Values shown represent mRNA expression levels in experimental cells relative to control cells. Data represent the mean±s.d. of three independent experiments using Huh7 cells. *$P<0.05$ (*t*-test). Similar results were obtained for PLC/PRF/5 cells. (**c**) The degree of cell migration was characterized using a scratch assay. The ratio of migrating cells was significantly increased in miR122-silenced cells at 24 and 48 h after scratching. Left panels show representative images. Right panel shows the results from cell counts for four randomly chosen fields per experiment. Data are represented as the mean±s.d. of three experiments using Huh7 control (solid line) and miR122-silenced cells (dashed line). *$P<0.001$ (*t*-test). Similar results were obtained for PLC/PRF/5 cells. (**d**) The degree of cell invasion was examined using cell invasion chambers. Representative images of stained invaded cells (left). The relative cell invasion ratio after normalization to control cell invasion levels (right). Data represent the mean±s.d. of three independent experiments using Huh7 cells. Scale bar, 100 μm. *$P<0.01$ (*t*-test). Similar results were obtained for PLC/PRF/5 cells. (**e**) Rho and Rac1 activity was determined by comparing the amounts of active GTP-bound RhoA (RhoA-GTP) and Rac1 (Rac1-GTP) between control and miR122-silenced cells. The indicated numbers represent the relative expression levels. Equal loading in pull-down assays was confirmed by analysis of β-actin levels in the cell lysates. Representative results of five independent experiments using Huh7 cells are shown. Similar results were obtained using PLC/PRF/5 cells.

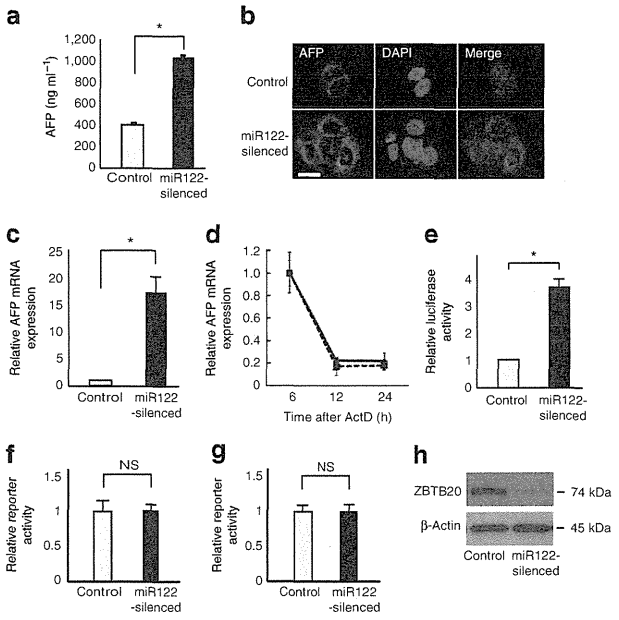

Figure 3 | Increased expression of AFP in HCC cells silenced for miR122 function. (**a**) The AFP concentration in the culture medium was determined by ELISA. Data represent the mean±s.d. of three independent experiments using Huh7 cells. $^*P<0.01$ (*t*-test). Similar results were obtained for PLC/PRF/5 cells. (**b**) Immunofluorescent staining for AFP in the cytoplasm of control and miR122-silenced Huh7cells. Representative images of stained cells from three independent experiments are shown. Scale bar, 50 μm. (**c**) Amounts of AFP mRNA in Huh7 control and miR122-silenced cells were determined by quantitative RT-PCR. Data represent the mean±s.d. of three independent experiments. $^*P<0.05$ (*t*-test). Similar results were obtained using PLC/PRF/5 cells. (**d**) AFP mRNA stability in Huh7 control (solid line) and miR122-silenced (dashed line) cells was determined by quantitative RT-PCR at 6, 12, and 24 h after treating cells with 10 μl ml^{-1} actinomycin D. Data represent the mean±s.d. of three independent experiments. Similar results were observed using PLC/PRF/5 cells. (**e**) AFP promoter activity was measured in reporter assays using Huh7 cells and AFP promoter-luciferase construct. Data represent the mean±s.d. of three independent experiments. $^*P<0.05$ (*t*-test). Similar results were obtained using PLC/PRF/5 cells. (**f**, **g**) Luciferase assays were performed using reporter plasmids to measure p53 (**f**) and β-catenin (**g**) activities. Data represent the mean±s.d. of three independent experiments. Similar results were obtained using PLC/PRF/5 cells. (**h**) ZBTB20 protein levels in miR122-silenced cells. A representative result from three independent experiments using Huh7 cells is shown. Similar results were obtained using PLC/PRF/5 cells.

in miR122-silenced cells as a result of increased AFP promoter activity. Indeed, AFP promoter activity was almost four times higher in miR122-silenced cells than in control cells, as assessed by a reporter assay (Fig. 3e).

Because AFP promoter activity is in part regulated by p53 (ref. 7), we assessed p53 activity using reporter constructs. However, no changes in p53 activity were detected in miR122-silenced cells (Fig. 3f). As mutation of β-catenin has also been reported to be involved in upregulation of AFP expression[8], we next analysed β-catenin activity in miR122-silenced cells. Similar to p53, no change in β-catenin activity was evident in miR122-silenced cells compared with control cells (Fig. 3g).

Recently, it was reported that ZBTB20 acts as a repressor of AFP transcription[9]. This result led us to assess the expression of the ZBTB20 protein in miR122-silenced cells. Indeed, western blot analysis revealed that ZBTB20 expression was decreased in miR122-silenced cells (Fig. 3h). However, as ZBT20 lacks the presence of predicted miR122 target sequences based on computational searches of the 3′-UTR, it was also unlikely that miR122 directly regulates ZBTB20 expression. These observations suggest that other indirect mechanisms may lead to decreased ZBTB20 expression in miR122-silenced cells.

CUX1 is the regulator of phenotypes in miR122-silenced cells. To explore the mechanisms by which miR122 regulates cell motility, invasion and AFP expression, we used computational searches to identify potential miR122 target genes with known functions related to these processes. This analysis led to the identification of Cut homeobox 1 (CUX1, also known as CCAAT-displacement protein/cut homeobox, CDP/Cux/Cut) through the presence of a high probability miR122 target site located in the 3′-UTR and a perfect match in the seed sequences. CUX1 is a transcription factor that regulates multiple processes including cell cycle progression, chromosomal segregation and cell migration[29,30]. Consistent with the effects of miR122 silencing described above, CUX1 was reported to modulate cell motility and invasion through the control of RhoA activity[31–33]. We observed that whereas CUX1 mRNA levels remained unchanged (Fig. 4a), there was a significant increase in the steady-state level of the CUX1 p200 and p110 isoforms in miR122-silenced cells (Fig. 4b).

To investigate the contribution of CUX1 upregulation to the increase in AFP expression and invasive properties observed in miR122-silenced cells, we knocked down CUX1 protein expression using lentiviruses expressing CUX1 short hairpin RNAs (shRNAs) (Fig. 4c). In the resulting double-knockdown cells, AFP protein expression in cell-culture supernatant and cell invasion were both reduced to levels similar to that of the parental Huh7 cells (Fig. 4d–f).

CUX1 represses ZBTB20 expression via miR214. We next assessed whether miR122 directly targets CUX1 by constructing a luciferase reporter construct that possessed a portion of the CUX1 3′-UTR containing the putative miR122 target site (Fig. 5a). Co-transfection experiments revealed that luciferase activity was suppressed by overexpression of a miR122 precursor-expressing plasmid (Fig. 5b). This suppressive effect was prevented by introducing two point mutations into the seed sequences of the miR122 target site (Fig. 5a,b), demonstrating that miR122 directly targets these sequences.

To confirm these effects, we generated 293T cell lines that stably expressed the miR122-precursor construct by transducing cells with miR122 precursor-expressing lentiviruses tagged with green fluorescent protein (Supplementary Fig. S2a). As expected, the anti-miR122 construct did not affect control 293T cells, owing to the lack of miR122 expression. However, the anti-miR122 construct greatly enhanced luciferase activity in 293T cells stably expressing the miR122-precursor, confirming that miR122 was transduced into the 293 T cells (Supplementary Fig. S2b). Consistent with the results described above, these cells exhibited decreased expression of CUX1, particularly the p200 isoform, and also showed a modest, but reproducible, increase in ZBTB20 expression (Fig. 5c). These results suggest that miR122 directly regulates CUX1 protein expression, which in turn may regulate ZBTB20 expression.

Because CUX1 can function as a transcriptional modulator[29], we initially hypothesized that CUX1 is a direct regulator of ZBTB20 transcription. However, quantitative RT–PCR analysis revealed that levels of the ZBTB20 mRNA were unchanged in miR122-silenced cells compared with controls (Fig. 5d). To explain the discrepancy between unchanged levels of ZBTB20 mRNA and decreases in protein expression levels in miR122-silenced cells, we searched for miRNAs that could potentially target the ZBTB20 3′-UTR. Based on computational searches, miR214 and miR375 were identified as candidate ZBTB20-regulatory miRNAs. Although levels of miR375 were unchanged in miR122-silenced cells (Fig. 5e), expression of miR214 was significantly increased (Fig. 5e).

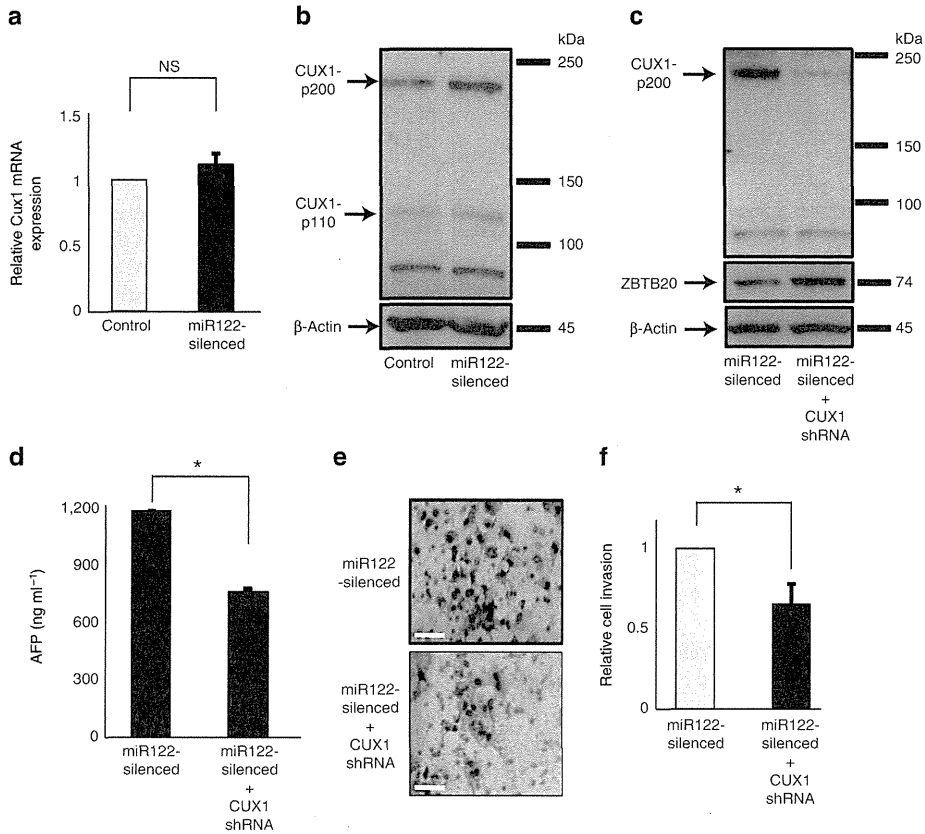

Figure 4 | CUX1-mediated regulation of AFP expression and phenotypic changes in miR122 functionally silenced cells. (**a**) CUX1 mRNA levels in control and miR122-silenced cells were analysed by quantitative RT-PCR. Data represent the mean±s.d. of three independent experiments using Huh7 cells. (**b**) p200 and p110 CUX1 protein levels were increased in miR122-silenced cells compared with control cells. A representative result from three independent experiments using Huh7 cells is shown. Similar results were obtained for PLC/PRF/5 cells. (**c**) CUX1 and ZBTB20 protein expression in double CUX1/miR122 knockdown Huh7 cells. Similar results were obtained using PLC/PRF/5 cells. (**d**) AFP concentrations in the culture medium supernatants were determined by ELISA. Data represent the mean±s.d. of three independent experiments. *$P<0.01$ (*t*-test). Similar results were observed using PLC/PRF/5 cells. (**e**, **f**) The change of cell invasion ratio by CUX1 knockdown in miR122-silenced Huh7 cells. Representative images of stained invading cells are shown (**e**). The relative cell invasion ratio after normalization to control invasion levels is shown (**f**). Data represent the mean±s.d. of three independent experiments. Scale bar, 100 μm. *$P<0.01$ (*t*-test). Similar results were obtained using PLC/PRF/5 cells.

To assess whether miR214 directly targeted the ZBTB20 3′-UTR, we constructed a luciferase reporter with the region of the ZBTB20 3′-UTR that contains the putative miR214 target site. Reporter assays revealed that luciferase activity was indeed suppressed by overexpression of the miR214 precursor, suggesting that miR214 directly targets the ZBTB20 3′-UTR and suppresses its expression (Fig. 5f). Consistent with these findings, cells that stably overexpressed the miR214 precursor exhibited decreased levels of ZBTB20 protein expression (Fig. 5g).

The putative promoter regions of miR214 contain multiple CUX1 binding sites as revealed by MATCH, a transcription factor binding site search engine (http://www.gene-regulation.com). A scanning chromatin immunoprecipitation (ChIP) experiment, followed by real-time PCR, using a series of primer pairs, confirmed that CUX1 binds to multiple genomic sites in the miR214 promoter region (Fig. 6a). We therefore hypothesized that CUX1 may regulate miR214 transcription. Consistent with this notion, we found that miR214 expression was decreased in CUX1 knockdown Huh7 cells (Fig. 6b). The role of CUX1 as an activator of miR214 transcription was further verified by knocking down or overexpressing CUX1 in another cell line. Levels of miR214 decreased following the constitutive knockdown of CUX1 with shRNA (Fig. 6c). In contrast, retroviral infection with a vector expressing p110 CUX1 led to an increase in miR214 (Fig. 6d). These findings were confirmed using doxycycline-inducible CUX1 shRNA. As previously observed for other transcriptional targets of CUX1 (refs 30,34), levels of miR214 were reduced in the presence of doxycycline, and then returned to levels higher than in untreated cells upon removal of the doxycycline inducer miR214 (Fig. 6e).

Next, to assess the contribution of miR214 to the control of ZBTB20 expression in miR122-silenced cells, we measured ZBTB20 expression after parallel silencing of miR214 in miR122-silenced cells. Although ZBTB20 protein expression was reduced by almost 50% by miR122 silencing, it was restored to >90% of control levels by miR214 silencing (Supplementary Fig. S3). Thus, CUX1-induced miR214 regulates, at least in part, ZBTB20 expression in miR122-silenced cells, leading to the upregulation of AFP expression.

Regulation of of CUX1 and AFP expression by miR122 was also confirmed in other HCC cell lines in which miR122 was overexpressed or silenced. Northern blotting showed that the expression of miR122 was relatively low in Hep3B and HepG2 cells, but was relatively high in Huh1, Huh7 and PLC/PRF/5 cells (Supplementary Fig. S4a). We therefore overexpressed the miR122 precursor in Hep3B and HepG2 cells and silenced miR122 in Huh1, Huh7 and PLC/PRF/5 cells (Supplementary Fig. S4b). CUX1 expression was respectively suppressed and enhanced by miR122 precursor overexpression and miR122 silencing (Supplementary Fig. S4c). In contrast, AFP expression was respectively enhanced and suppressed

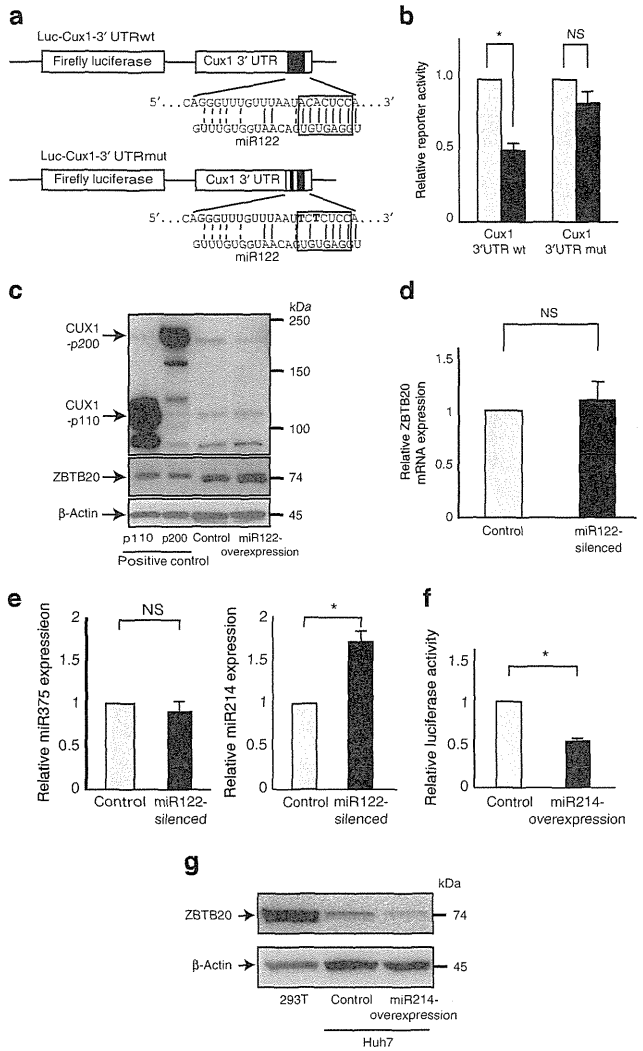

Figure 5 | MiR122 directly targets CUX1. (**a**) A luciferase reporter carrying a region of the wild type CUX1 3′UTR containing the putative miR122 target site (Luc-CUX1-3′UTRwt) was used to assess the effects of miR122 on expression of CUX1. A second luciferase reporter with two nucleotide mutations (indicated in bold) in the seed sequences (indicated by a rectangle) of the putative miR122 target sites (Luc-CUX1-3′UTRmut) was also utilized to assess specificity. (**b**) Huh7 cells were co-transfected with Luc-CUX1-3′UTRwt or Luc-CUX1-3′UTRmut and either an empty control vector (white bar) or a miR122 precursor expression plasmid (black bar). Data represent the mean±s.d. of three independent experiments. *$P<0.05$ (*t*-test). (**c**) CUX1 and ZBTB20 expression in 293T cells-expressing the miR122 precursor. Cell lysates transiently transfected with CUX1 p200 or p110 expression plasmids were used as positive controls. Representative results from four independent experiments are shown. (**d**) ZBTB20 mRNA levels in miR122-silenced Huh7 cells were determined by quantitative RT-PCR. Data represent the mean±s.d. of three independent experiments. Similar results were obtained using PLC/PRF/5 cells. (**e**) Levels of miR375 (left) and miR214 (right) in miR122-silenced Huh7 cells were analysed by quantitative RT-PCR. Data represent the mean±s.d. of three independent experiments. *$P<0.05$ (*t*-test). (**f**) Huh7 cells were co-transfected with Luc-ZBTB20-3′UTR and either an empty control vector or an miR214 precursor expression plasmid. Data represent the mean±s.d. of three independent experiments. *$P<0.05$ (*t*-test). (**g**) ZBTB20 expression was decreased in Huh7 miR214-overexpressing cells. 293T cell lysate was used as a positive control. Representative results from four independent experiments are shown.

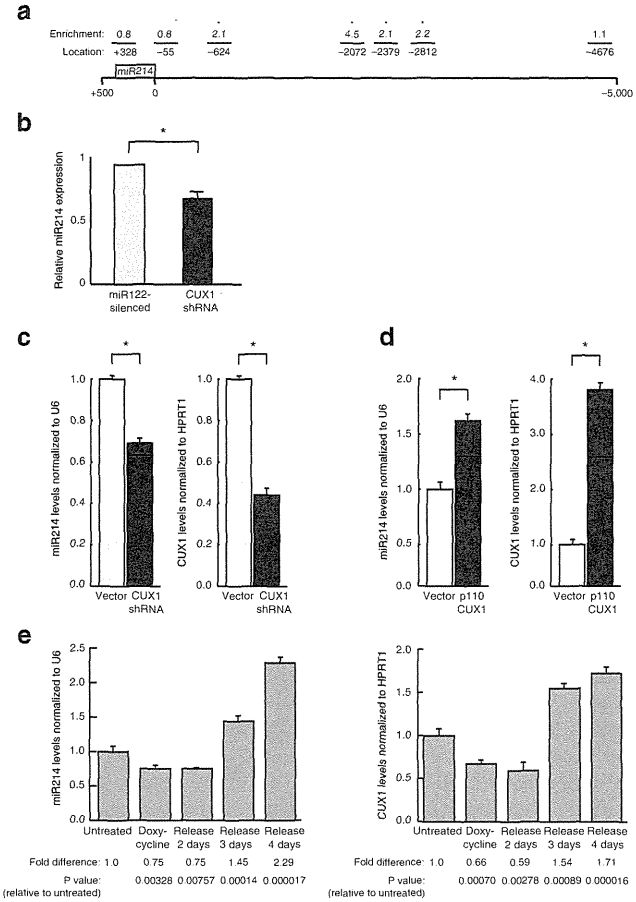

Figure 6 | CUX1 regulated miR-214 expression. (**a**), CUX1 enrichment at the miR214 locus. ChIP assays were performed using Hs578T cells. Fold enrichment and location of the center of each qPCR amplicon are shown. *$P<0.05$ (*t*-test). (**b**) MiR214 expression levels after CUX1 knockdown in miR122-silenced Huh7 cells were determined by quantitative RT-PCR. Data represent the mean±s.d. of three independent experiments. *$P<0.05$ (*t*-test). Similar results were obtained using PLC/PRF/5 cells. (**c**) Levels of miR214 and CUX1 RNA in Hs578T cells infected with an empty vector or a lentiviral vector constitutively expressing CUX1 shRNA. Data represent the mean±s.d. of three independent experiments. *$P<0.05$ (*t*-test). (**d**) Hs578T cells were infected with a retrovirus expressing p110 CUX1. Levels of miR214 and CUX1 mRNA were measured 1 day later. Data represent the mean±s.d. of three independent experiments. *$P<0.05$ (*t*-test). (**e**) Levels of miR214 and CUX1 mRNA in Hs578T cells expressing a doxycycline-inducible CUX1 shRNA. Levels are shown prior to treatment, after 5 days of doxycycline treatment, and 2, 3 and 4 days after withdrawal of doxycycline. Fold changes with the mean±s.d. of three independent experiments and *P*-values are shown (*t*-test).

(Supplementary Fig. S4d), confirming that AFP expression is regulated by an miR122-CUX1 pathway in multiple HCC cell lines.

These results indicate that functional silencing of miR122 leads to an increase in CUX1 protein expression, resulting in repression of ZBTB20 through an increase in miR214 expression. Repression of ZBTB20, in turn, leads to an increase in AFP expression. Because CUX1 is a modulator of cell motility and invasion[35–37], upregulation of this protein also enhances RhoA activity, increasing the malignant properties of cancer cells.

Expression of CUX1-related molecules in miR122-silenced mice. To explore the pathway delineated above in an *in vivo* model, we gen-

erated transgenic mice expressing antisense miR122 under the control of an H1 promoter (Fig. 7a) to inhibit the function of endogenous miR122 (ref. 38). *In situ* hybridization analysis in these mice revealed weak miR122 staining in liver tissue in comparison with control mice, likely due to binding of the anti-sense miR122 to endogenous miR122, which produces a double-stranded DNA and likely inhibits hybridization of the probe (Fig. 7b). Although structural development of the liver appeared normal based on haematoxylin and eosin staining (Supplementary Fig. S5), AFP mRNA expression (Fig. 7c) and p200 and p110 CUX1 protein expression were upregulated in the liver of anti-miR122 transgenic mice (Fig. 7d). Moreover, whereas levels of ZBTB20 mRNA were unchanged, ZBTB20 protein expression was decreased in the liver (Fig. 7d), in agreement with *in vitro* results demonstrating the regulation of ZBTB20 at the translational level (Fig. 5c,d). This was associated with a significant increase in the levels of miR214 in anti-miR122 transgenic mice (Fig. 7e). Thus, results from mouse liver tissue confirm that the miR122/CUX1/miR214/ZBTB20 regulatory pathway is also functional in an *in vivo* model.

Invasiveness of miR122-silenced cells in xenograft model. Next, we transplanted control and miR122-silenced PLC/PRF/5 cells under the liver capsule of nude mice (Fig. 7f) to determine whether miR122 silencing in HCC actually produces a more malignant phenotype *in vivo*. PLC/PRF/5 cells were chosen because of their transplantability in nude mice[39]. Neither intrahepatic metastases nor vascular invasion were detected in the livers of mice transplanted with control cells at 4 weeks post-transplantation. In contrast, vascular invasion was observed in the livers of mice transplanted with miR122-silenced HCC cells (Fig. 7g). These results suggest that miR122 silencing in HCC leads to a more aggressive phenotype.

HCC staging and the expression of miR122-related molecules. To assess the relevance of these results to human disease, we examined miR122 and AFP expression in several clinical-grade human HCC samples. We analysed miR122 expression by *in situ* hybridization (Fig. 8a) and AFP expression by immunohistochemistry (Fig. 8b). Both AFP expression and malignancy grading were inversely correlated with miR122 expression levels (Fig. 8c,d). In addition, CUX1, miR214 and ZBTB20 expression was also correlated with miR122 expression, as determined using serial sections (Supplementary Fig. S6a, b and c). These results, together with our studies in tissue culture systems and a transgenic mouse model, suggest that a reduction in the expression of miR122 increases AFP expression via a miRNA122-CUX1-miRNA214-ZBTB20 pathway and that the development of more biologically aggressive forms of HCC occurs via a miRNA122-CUX1-RhoA pathway (Supplementary Fig. S7). The miRNA-mediated mechanism described in this report may explain the clinically known link between increased AFP levels and more biologically aggressive cell characteristics in HCC.

Discussion

High AFP levels have been clinically shown to be an unfavourable prognostic factor in HCC patients[40]. In this study, we demonstrate that reduced expression of miR122 in HCC cells contributes to elevated AFP expression and, subsequently, a more aggressive phenotype. These results provide a molecular framework that explains the reported link between elevated AFP levels and a poor clinical outcome in HCC patients.

Clinically, high AFP expression is correlated with more biologically aggressive properties of HCC, as patients with high AFP levels have a significantly higher frequency of portal vein invasion and intrahepatic metastases. Additionally, these patients display significantly lower rates of recurrence-free survival and a trend towards lower overall survival[41]. In the present study, we have presented several lines of evidence indicating that decreased expression of miR122 in HCC leads to the two phenomena that

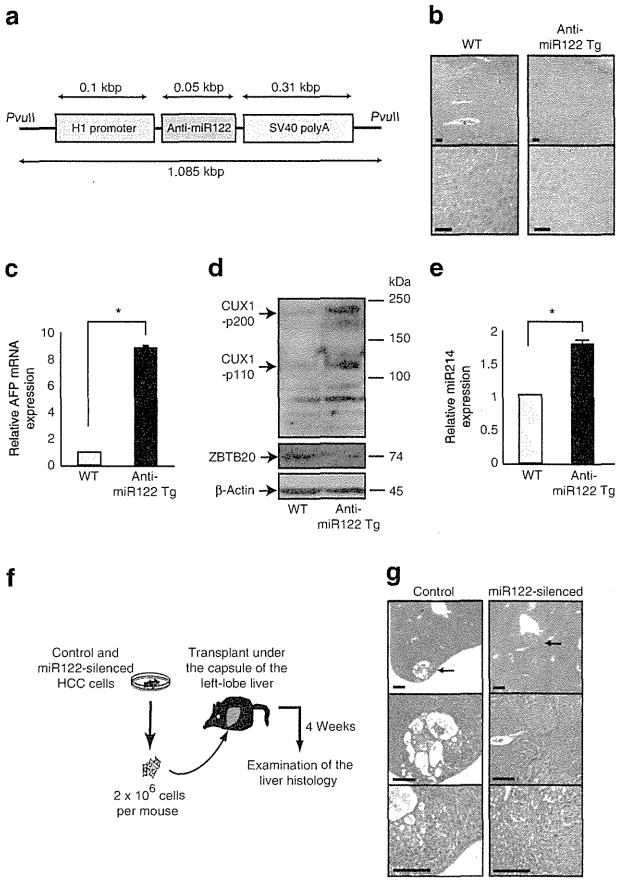

Figure 7 | AFP expression is increased in the liver of anti-miR122 transgenic mice. (**a**) DNA construct used to establishment transgenic mice in which miR122 is functionally silenced (anti-miR122 transgenic mice). This construct (like the construct used in the *in vitro* studies) generates a functional single-stranded full-length antisense miRNA complementary to miR122. (**b**) Confirmation of the expression of an antisense RNA directed against miR122 in anti-miR122 transgenic (anti-miR122 Tg) mice. Amounts of miR122 detected by *in situ* hybridization (blue/purple staining) in the liver tissues of anti-miR122 transgenic mice and WT mice. Results shown are representative of three independent experiments performed using littermates from four different mouse lines. Scale bar, 100 μm. No specific staining was observed when a negative control probe (LNA-scramble) was used. (**c**) AFP mRNA expression in mouse liver tissues was analysed by quantitative RT-PCR. Data represent the mean±s.d. of results for five mice in each group. $^*P<0.05$ (*t*-test). (**d**) CUX1 and ZBTB20 expression in mouse liver tissues was assessed by Western blotting. A representative result from three independent experiments is shown. (**e**) Levels of miR214 in liver tissues were determined by quantitative RT-PCR. Data represent the mean±s.d. of three independent experiments. $^*P<0.05$ (*t*-test). (**f**) Protocols of the orthotopic xenograft models of HCC cells. Control and miR122-silenced PLC/PRF/5 cells were prepared and injected under the capsule of the left-lobe of the nude mouse liver. Six mice were included in each group. At 4 weeks after transplantation, liver tissues were collected and sliced in series. Histological examination by H&E staining was performed to examine the tumour cell invasion status. (**g**) Representative liver histology images at 4 weeks after transplantation of tumour cells are shown. Whereas only the transplanted HCC cells beneath the capsule of the liver edge could be detected (arrow, upper left panel), neither intrahepatic metastasis nor vascular invasion was observed in the livers of mice transplanted with control cells. In contrast, vascular invasion by multiple tumour cells (arrow, upper right panel) was observed in mice transplanted with miR122-silenced cells. Scale bar, 500 μm. WT, wild type.

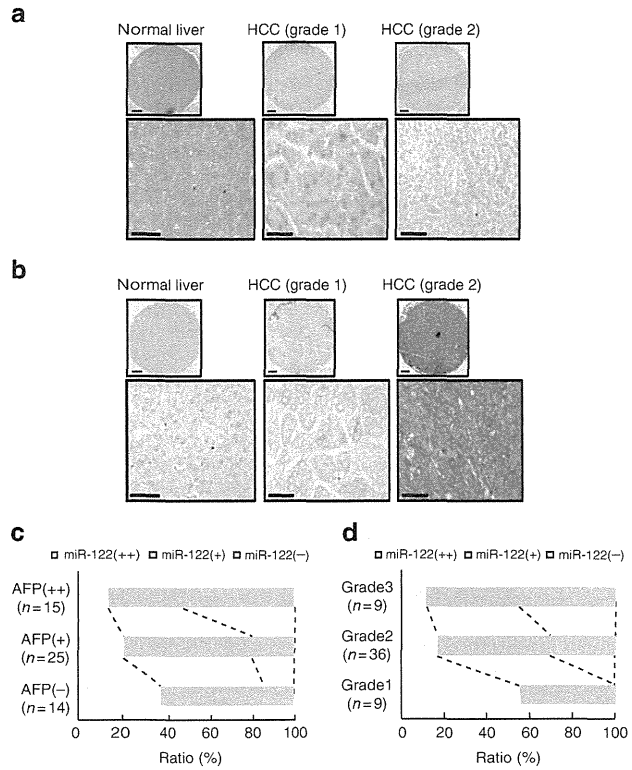

Figure 8 | AFP expression and HCC grade are inversely correlated with miR122 expression in human HCC samples. (**a**) Expression of miR122 in human clinical samples was assessed by *in situ* hybridization. Expression of miR122 (blue/purple staining) in grade 2 (more malignant) HCC samples was less than that of normal human liver tissues or grade 1 (less malignant) HCC samples. Representative images are shown. Nuclei were stained with FastRed. Scale bar, 500 μm. (**b**) AFP expression, shown in brown, was analysed by immunohistochemistry. AFP expression was higher in grade 2 HCC samples than in normal human liver tissue or grade 1 HCC samples in most cases. Representative images are shown. Scale bar, 500 μm. (**c**) Graph shows the correlation between miR122 and AFP expression. Increased AFP expression was correlated with decreased miR122 expression. (**d**) Graph shows the correlation between miR122 expression and malignancy grading of HCC. Increases in malignancy grading were correlated with decreases in miR122 expression.

are frequently observed simultaneously in the clinic: elevated expression of AFP and a more malignant biological phenotype. First, elevated AFP expression and greater cellular invasiveness were observed in miR122-knockdown cells *in vitro* and *in vivo*. Second, CUX1, which is linked with invasive characteristics in carcinoma cells[32,36,37], was shown to be involved in regulation of AFP expression and was identified as a direct target of miR122. Third, in human tissue samples from HCC patients, inverse correlations were observed between miR122 expression and AFP expression, and between miR122 expression and tumour grade. These data suggest that it is unlikely that the clinical correlation between elevated AFP levels and a more biologically aggressive phenotype in HCC is a coincidental epiphenomenon, but, instead provide a possible molecular explanation for the decrease in miR122 expression in HCC cells.

A recent study on liver development reported that liver-enriched transcription factors activate the expression of miR122, which in turn was found to promote terminal differentiation of hepatocytes through the silencing of CUX1 (ref. 42). In the present study, we confirmed that CUX1 is a direct target of miR122 and, in contrast to the situation in normal development, we showed that in grade 2 HCCs the decrease in miR122 is associated with higher CUX1 expression. High CUX1 expression was previously shown to inversely correlate with relapse-free and overall survival in high-grade breast cancers[36]. In transgenic mice, CUX1 was reported to cause various cancer-associated disorders depending on the specific isoform and tissue type expression[34,43–46]. In particular, expression of CUX1 caused organomegaly in several organs including the liver[43]. Hepatomegaly was associated with progression of lesions beginning with inflammation and leading to the development of mixed cell foci, hyperplasia and even HCCs, although in this last case statistical significance was not achieved because of the small size of the transgenic cohort[47]. The underlying mechanisms for the role of CUX1 in cancer is complex and is likely to involve both cell-autonomous and non-cell autonomous effects. However, from cell-based assays it is clear that CUX1 has a role in at least three distinct processes: cell motility, cell cycle progression and chromosome segregation[30,31,36,48]. The knockdown of CUX1 using siRNA was shown to delay entry into S phase and to hinder cell motility and invasion[31,36,48]. In contrast, overexpression of p110 CUX1 was able to accelerate S phase entry and to stimulate proliferation, migration and invasion[35,48]. Moreover, CUX1 was shown to promote genomic instability following cytokinesis failure[30]

Regulation of AFP gene expression is a complex process mediated by a number of transcriptional activators and repressors that bind the AFP gene[7,8]. ZBTB20 was recently identified as a potent repressor of AFP transcription in knockout mouse studies[9]. Our results demonstrate that decreased miR122 expression leads to concomitant decreases in ZBTB20 protein expression. This effect is mediated through upregulation of CUX1, as CUX1 silencing in miR122-silenced cells was shown to lead to both recovery of ZBTB20 levels and reduced AFP expression. Furthermore, the increased expression level of ZBTB20 in CUX1 knockdown cells suggests that ZBTB20 expression is regulated by CUX1. This miR122/CUX1/miR214/ZBTB20/AFP pathway may explain the deregulated AFP expression observed in HCC cells. Additionally, the ability of CUX1 to activate RhoA and to regulate the expression of many proteins involved in cell motility may explain the increased migration and invasiveness associated with malignancy of HCC[31–36]. It should be noted that, although this analysis revealed a trend toward inverse correlation between expression of miR122 and expression of AFP, this correlation could not be applied to all cases examined. Therefore, the possibility of additional pathways that regulate AFP expression cannot be discounted. Nonetheless, our results demonstrate that a decrease in miR122 function is a key factor that contributes to the regulation of AFP expression in HCC.

MiR122 is the most abundant miRNA in the normal adult liver, comprising approximately 80% of all miRNAs[18]. The numerous reported roles of miR122 include regulation of cholesterol biosynthesis[19,20], hepatitis C virus replication[49] and maintenance of the adult liver phenotype[21]. Specific miRNAs are often involved in the differentiation of specific cells and tissues[50]. As miR122 is liver-specific, we reasoned that this miRNA may have a role in the differentiation of normal hepatocytes. In our study, transgenic mice in which miR122 was functionally silenced were found to exhibit elevated AFP levels, but did not display abnormal morphological development in the liver (at least, not up to the age of 12 weeks), suggesting that decreased miR122 expression itself does not cause cells to become transformed. Ongoing characterization of these mice will be required to fully determine the physiological roles of miR122 in the noncancerous liver *in vivo*.

In summary, we have shown that decreased miR122 expression in HCC is linked both to more biologically aggressive tumour behaviour and elevated AFP expression. Furthermore, both of these effects were shown to be mediated by increased expression of CUX1, a direct target of miR122. Similar strategies could also be used to develop new therapeutics and diagnostics for other cancers in which miRNAs that regulate both tumour characteristics and serum markers have been identified.

Methods

Cell culture. The human HCC cell lines, Huh7, PLC/PRF/5, HepG2, Hep3B and Huh1 were obtained from the Japanese Collection of Research Bioresources. The human embryonic kidney cell line, 293T and the human breast cancer cell line HS578T were obtained from the American Type Culture Collection . All cells were maintained in Dulbecco's modified Eagle medium, supplemented with 10% fetal bovine serum.

Mouse experiments. All experiments were carried out in compliance with the regulations of the Animal Use Committee of The University of Tokyo and The Institute for Adult Disease, Asahi Life Foundation.

Generation of transgenic mice in which miR122 was functionally silenced. Mice in which miR122 function was knocked down were generated using previously described protocols[38,51]. Briefly, a DNA fragment of 1,085 bp, containing the H1 promoter region, the coding region for the antisense miR122 stem-loop-stem RNA precursor, and a transcriptional terminator of five thymidines, was resected from the miRZip-122 construct described above by digestion with *Pvu*II. Proper silencing function of the resulting DNA was confirmed via transient transfection-based reporter assays that showed efficient knockdown of miR122 function. Stable C57BL/6 embryonic stem cell lines were generated by electroporation of the linearized transgene, and the resulting cells were injected into blastocysts by the UNITECH Company. Genotyping was performed by PCR using DNA isolated from tail snips. Four different mouse lines were maintained and the male littermates were used in experiments.

Chromatin immunoprecipitation assay. ChIP for CUX1 was performed as previously described[52]. For the scanning ChIP of the miR214 locus, realtime PCR analysis was performed using primer pairs specific for different regions of the promoters. Templates for the PCR reactions were 0.1% total input DNA (I), nonspecific DNA from sepharose beads alone (S), or chipped chromatin. The respective fold enrichment of the different DNA fragments are indicated relative to the DNA obtained by purification on sepharose beads without IgG (S). Enrichment was calculated using the HPRT locus as a reference.

Doxycyclin-induced shRNA against CUX1 system. For conditional knockdown of CUX1 in Hs578t cells, we took advantage of the Addgene plasmid 11643. HS578T cells were infected with pLVCT shCUX1(5,326–5,348)-tTRKRAB lentivirus as described[53]. At 48 h after infection, cells were split and cultured with or without doxycyclin at a final concentration of 2.5 $\mu g\,ml^{-1}$. Cells were used for experiments after 5 days of treatment. Doxycyclin was then removed from the culture media and cells were maintained for 4 days following release.

Cell proliferation assay. Relative cell proliferation was assessed using a Cell Counting Kit-8 (Dojindo Laboratories), as described previously[54].

Enzyme-linked immunosorbent assay. AFP levels in the cell-culture supernatant were examined using an AFP-specific ELISA kit supplied by an outsourcing company, SRL.

Western blot analysis. Protein lysates were prepared from cells or mouse liver for immunoblot analysis. Proteins were separated by SDS–polyacrylamide gel electrophoresis and transferred to polyvinylidene difluoride membranes. After blocking with 5% dry milk to decrease nonspecific binding, membranes were probed with the appropriate primary antibodies. Primary antibodies were obtained from Abcam (ZBTB20, #ab48889, 1:500) and Santa Cruz Biotechnology (CDP, #sc-13024, 1:1,000). CUX1 antibodies (#861, 1:1,000) were generated as described previously[52]. Horseradish peroxidase-conjugated secondary antibodies were used to detect primary antibodies. Bound antibodies were detected using ECL Plus Western blotting detection reagents (GE Healthcare Life Sciences).

Scratch assay. The effects of miR122 knockdown on cellular migratory function were determined by evaluating cellular migration after scratching of a confluent monolayer of cells. Monolayers were cultured on 10 $\mu g\,ml^{-1}$ fibronectin-coated dishes and were scratched using a 200-µl pipette. Migration was analysed at the indicated time points after scratching.

***In vitro* invasion assay**. The effect of miR122 knockdown on invasive function was determined using BD BioCoat Matrigel Invasion Chambers (Becton Dickinson) according to the manufacturer's recommended protocol. Cell invasion was induced by removing the serum in the upper chamber. The number of invading cells was analysed after 22-h incubation. Cell numbers were counted in four randomly chosen fields at each time point.

Quantitative pseudopodia assay. Pseudopodium quantitation was performed using a Quantitative Pseudopodia Assay Kit (Chemicon) according to the manufacturer's instructions. Briefly, the upper chamber was coated with fibronectin and seeded with cells in serum-free medium. Serum was added to the lower chambers. 8 h later, pseudopodia on the lower surface were stained and eluted, and the absorbances of solubilized samples at 600 nm was measured using a microplate reader.

CUX1-knockdown lentiviral construct. Lentiviral particles expressing CUX1 shRNA were purchased from Santa Cruz Biotechnology (#sc-35051-V).

***In situ* hybridization to assess miR122 and miR214**. The expression of miR122 and miR214 in mouse liver and human HCC tissues was examined by *in situ* hybridization[55,56]. Locked nucleic acid (LNA)-scramble (negative control) and LNA-anti-miR122 and LNA-anti-miR214 probes were obtained from EXIQON. After deparaffinization, tissue sections were treated with 10 $\mu g\,ml^{-1}$ proteinase K for 5 min at 37 °C and refixed with 4% paraformaldehyde, followed by acetylation with 0.25% anhydrous acetic acid in 0.1 M Tris–HCl buffer (pH 8.0). Following pre-hybridization for 30 min at 48 °C, hybridization was performed overnight with each 20 nM LNA probe in hybridization buffer (5xSSC buffer, 50% formamide, 500 $\mu g\,ml^{-1}$ tRNA, 50 $\mu g\,ml^{-1}$ Cot-1 DNA). After completion of hybridization, the sections were washed with 0.1×SSC buffer for 10 min at 52 °C three times and blocked with DIG blocking buffer (Roche Diagnostics) for 30 min. Sections were then probed with anti-DIG (1:500; Roche Diagnostics) for 1 h at room temperature. Detection was performed by incubation in NBT/BCIP buffer (Promega) overnight. Nuclei were stained with Nuclear FastRed (Sigma-Aldrich).

Immunohistochemistry. Tissue arrays containing HCC tissues were purchased from US Biomax. To determine the correlations between AFP, ZBTB20, CUX1, miR122 and miR214 expression and HCC differentiation grade, slides carrying consecutive sections were obtained. Slides were baked at 65 °C for 1 h and deparaffinized. Endogenous peroxidase activity was blocked by incubation in 3% hydrogen peroxide buffer for 30 min. Antigen retrieval was performed by incubating the slides at 89 °C in 10 mM sodium citrate buffer (pH 6.0) for 30 min. To minimize nonspecific background staining, slides were blocked in 5% normal goat serum (Dako) for 10 min at room temperature. Tissues were labelled overnight at 4 °C with primary antibodies raised against AFP (Dako, #N1501, 1:100), CUX1 (#sc-13024, 1:100) and ZBTB20 (HPA016815, Sigma-Aldrich, 1:100). Slides were then incubated with anti-rabbit horseradish peroxidase-conjugated secondary antibodies (Nichirei Bioscience) for 1 h. Primary antibody binding was visualized by incubation in 3,3′-diaminobenzidine in buffered substrate (Nichirei Bioscience) for 5 min. The slides were counterstained with haematoxylin, dehydrated with ethanol, and mounted with Clarion mounting medium (Biomeda).

GTP-binding RhoA and Rac1 immunoprecipitation assay. The amount of RhoA activity was examined using an Active Rho Pull-down and Detection Kit (Thermo Fisher Scientific) according to the manufacturer's recommended protocol. The amount of GTP-bound RhoA protein (the active form of RhoA) was detected by Western blotting with the provided anti-RhoA antibody (1:100). Rac1 activity was similarly determined by using PAK-GST Protein Beads (#PAK02, Cytoskeleton) for pulldowns and anti-Rac1 antibodies (1:100) for subsequent Western blotting (#89856D, Thermo Fisher Scientific).

Orthotopic xenograft tumour model of HCC. Male BALB/c (nu/nu) nude mice were purchased from CREA Japan (Tokyo, Japan). The transplantation of tumour cells into mouse livers was performed using previously reported methods[57,58]. Briefly, 2×10^6 control or miR122-silenced PLC/PRF5 cells were suspended in 30 µl of PBS containing 1% Matrigel (Becton Dickinson). After anaesthesia, the liver was exposed through a surgical incision. Cells were slowly injected under the capsule of left lobe of the liver using a 28-gauge needle. When successful, a transparent bleb of cells could be seen through the liver capsule. After injection, light pressure was applied to the injection site with sterile gauze for 2 min to prevent bleeding and tumour cell leakage. The abdomen was then closed with sutures. Transplantation was successful in a total of 12 mice (6/group). At 4 weeks post-transplantation, liver tissues were collected, serially sectioned, and stained with haematoxylin and eosin.

Statistical analysis. Statistically significant differences between groups were determined using Student's *t*-test when variances were equal. When variances were unequal, Welch's *t*-test was used instead. *P*-values less than 0.05 were considered statistically significant.

Plasmid and stable cell line construction, reporter assays, RT–PCR, northern blotting and immunocytochemistry are described in the Supplementary Methods. All primer information is provided in Supplementary Table S1.

References

1. Parkin, D., Bray, F., Ferlay, J. & Pisani, P. Global cancer statistics, 2002. *CA Cancer J. Clin.* **55,** 74–108 (2005).
2. El-Serag, H. Epidemiology of hepatocellular carcinoma in USA. *Hepatol. Res.* **37,** S88–94 (2007).
3. Llovet, J. *et al.* Sorafenib in advanced hepatocellular carcinoma. *N. Engl. J. Med.* **359,** 378–390 (2008).
4. Greten, T. *et al.* Survival rate in patients with hepatocellular carcinoma: a retrospective analysis of 389 patients. *Br. J. Cancer* **92,** 1862–1868 (2005).
5. Greten, T., Korangy, F., Manns, M. & Malek, N. Molecular therapy for the treatment of hepatocellular carcinoma. *Br. J. Cancer* **100,** 19–23 (2009).
6. Di Bisceglie, A. Issues in screening and surveillance for hepatocellular carcinoma. *Gastroenterology* **127,** S104–S107 (2004).

7. Ogden, S. *et al. p53* targets chromatin structure alteration to repress alpha-fetoprotein gene expression. *J. Biol. Chem.* **276,** 42057–42062 (2001).
8. Peng, S. *et al.* High alpha-fetoprotein level correlates with high stage, early recurrence and poor prognosis of hepatocellular carcinoma: significance of hepatitis virus infection, age, p53 and beta-catenin mutations. *Int. J. Cancer.* **112,** 44–50 (2004).
9. Xie, Z. *et al.* Zinc finger protein ZBTB20 is a key repressor of alpha-fetoprotein gene transcription in liver. *Proc. Natl Acad. Sci. USA* **105,** 10859–10864 (2008).
10. Oishi, K. *et al.* Clinicopathologic features of poorly differentiated hepatocellular carcinoma. *J. Surg. Oncol.* **95,** 311–316 (2007).
11. Yamamoto, K. *et al.* AFP, AFP-L3, DCP, and GP73 as markers for monitoring treatment response and recurrence and as surrogate markers of clinicopathological variables of HCC. *J. Gastroenterol.* **45,** 1272–1282 (2010).
12. Matsumoto, Y. *et al.* Clinical classification of hepatoma in Japan according to serial changes in serum alpha-fetoprotein levels. *Cancer* **49,** 354–360 (1982).
13. Lee, R., Feinbaum, R. & Ambros, V. The *C. elegans* heterochronic gene lin-4 encodes small RNAs with antisense complementarity to lin-14. *Cell* **75,** 843–854 (1993).
14. Carrington, J. & Ambros, V. Role of microRNAs in plant and animal development. *Science* **301,** 336–338 (2003).
15. Bartel, D. MicroRNAs: genomics, biogenesis, mechanism, and function. *Cell* **116,** 281–297 (2004).
16. Ambros, V. The functions of animal microRNAs. *Nature* **431,** 350–355 (2004).
17. Lu, J. *et al.* MicroRNA expression profiles classify human cancers. *Nature* **435,** 834–838 (2005).
18. Landgraf, P. *et al.* A mammalian microRNA expression atlas based on small RNA library sequencing. *Cell* **129,** 1401–1414 (2007).
19. Krützfeldt, J. *et al.* Silencing of microRNAs *in vivo* with 'antagomirs'. *Nature* **438,** 685–689 (2005).
20. Esau, C. *et al.* miR-122 regulation of lipid metabolism revealed by *in vivo* antisense targeting. *Cell Metab.* **3,** 87–98 (2006).
21. Gatfield, D. *et al.* Integration of microRNA miR-122 in hepatic circadian gene expression. *Genes Dev.* **23,** 1313–1326 (2009).
22. Yan, D. *et al.* MicroRNA-1/206 targets c-Met and inhibits rhabdomyosarcoma development. *J. Biol. Chem.* **284,** 29596–29604 (2009).
23. Kutay, H. *et al.* Downregulation of miR-122 in the rodent and human hepatocellular carcinomas. *J. Cell. Biochem.* **99,** 671–678 (2006).
24. Coulouarn, C., Factor, V., Andersen, J., Durkin, M. & Thorgeirsson, S. Loss of miR-122 expression in liver cancer correlates with suppression of the hepatic phenotype and gain of metastatic properties. *Oncogene* **28,** 3526–3536 (2009).
25. Tsai, W. *et al.* MicroRNA-122 a tumor suppressor microRNA that regulates intrahepatic metastasis of hepatocellular carcinoma. *Hepatology* **49,** 1571–1582 (2009).
26. Varnholt, H. *et al.* MicroRNA gene expression profile of hepatitis C virus-associated hepatocellular carcinoma. *Hepatology* **47,** 1223–1232 (2008).
27. Wong, Q. *et al.* MicroRNA-223 is commonly repressed in hepatocellular carcinoma and potentiates expression of Stathmin1. *Gastroenterology* **135,** 257–269 (2008).
28. Sahai, E. & Marshall, C. RHO-GTPases and cancer. *Nat. Rev. Cancer* **2,** 133–142 (2002).
29. Sansregret, L. & Nepveu, A. The multiple roles of CUX1: insights from mouse models and cell-based assays. *Gene* **412,** 84–94 (2008).
30. Sansregret, L. *et al.* Cut homeobox 1 causes chromosomal instability by promoting bipolar division after cytokinesis failure. *Proc. Natl Acad. Sci. USA* **108,** 1949–1954 (2011).
31. Kedinger, V. & Nepveu1, A. The roles of CUX1 homeodomain proteins in the establishment of a transcriptional program required for cell migration and invasion. *Cell Adh. Migr.* **4,** 348–352 (2010).
32. Michl, P., Knobel, B. & Downward, J. CUTL1 is phosphorylated by protein kinase A, modulating its effects on cell proliferation and motility. *J. Biol. Chem.* **281,** 15138–15144 (2006).
33. Seguin, L. *et al.* CUX1 and E2F1 regulate coordinated expression of the mitotic complex genes Ect2, MgcRacGAP, and MKLP1 in S phase. *Mol. Cell Biol.* **29,** 570–581 (2009).
34. Kedinger, V. *et al.* p110 CUX1 homeodomain protein stimulates cell migration and invasion in part through a regulatory cascade culminating in the repression of E-cadherin and occludin. *J. Biol. Chem.* **284,** 27701–27711 (2009).
35. Michl, P. *et al.* CUTL1 is a target of TGF(beta) signaling that enhances cancer cell motility and invasiveness. *Cancer Cell* **7,** 521–532 (2005).
36. Aleksic, T. *et al.* CUTL1 promotes tumor cell migration by decreasing proteasome-mediated Src degradation. *Oncogene* **26,** 5939–5949 (2007).
37. Kunath, T. *et al.* Transgenic RNA interference in ES cell-derived embryos recapitulates a genetic null phenotype. *Nat. Biotechnol.* **21,** 559–561 (2003).
38. Shouval, D. *et al.* Tumorigenicity in nude mice of a human hepatoma cell line containing hepatitis B virus DNA. *Cancer Res.* **41,** 1342–1350 (1981).
39. Nomura, F., Ohnishi, K. & Tanabe, Y. Clinical features and prognosis of hepatocellular carcinoma with reference to serum alpha-fetoprotein levels. Analysis of 606 patients. *Cancer* **64,** 1700–1707 (1989).
40. Johnson, P., Melia, W., Palmer, M., Portmann, B. & Williams, R. Relationship between serum alpha-foetoprotein, cirrhosis and survival in hepatocellular carcinoma. *Br. J. Cancer* **44,** 502–505 (1981).
41. Xu, H. *et al.* Liver-enriched transcription factors regulate microRNA-122 that targets CUTL1 during liver development. *Hepatology* **52,** 1431–1442 (2010).
42. Ledford, A. W. *et al.* Deregulated expression of the homeobox gene Cux-1 in transgenic mice results in downregulation of p27(kip1) expression during nephrogenesis, glomerular abnormalities, and multiorgan hyperplasia. *Dev. Biol.* **245,** 157–171 (2002).
43. Brantley, J. G., Sharma, M., Alcalay, N. I. & Heuvel, G. B. Cux-1 transgenic mice develop glomerulosclerosis and interstitial fibrosis. *Kidney Int.* **63,** 1240–1248 (2003).
44. Cadieux, C. *et al.* Mouse mammary tumor virus p75 and p110 CUX1 transgenic mice develop mammary tumors of various histologic types. *Cancer Res.* **69,** 7188–7197 (2009).
45. Cadieux, C. *et al.* Polycystic kidneys caused by sustained expression of Cux1 isoform p75. *J. Biol. Chem.* **283,** 13817–13824 (2008).
46. Cadieux, C. *et al.* Transgenic mice expressing the p75 CCAAT-displacement protein/Cut homeobox isoform develop a myeloproliferative disease-like myeloid leukemia. *Cancer Res.* **66,** 9492–9501 (2006).
47. Vanden Heuvel, G. B. *et al.* Hepatomegaly in transgenic mice expressing the homeobox gene Cux-1. *Mol. Carcinog.* **43,** 18–30 (2005).
48. Sansregret, L. *et al.* The p110 isoform of the CDP/Cux transcription factor accelerates entry into S phase. *Mol. Cell Biol.* **26,** 2441–2455 (2006).
49. Jopling, C., Yi, M., Lancaster, A., Lemon, S. & Sarnow, P. Modulation of hepatitis C virus RNA abundance by a liver-specific MicroRNA. *Science* **309,** 1577–1581 (2005).
50. Taulli, R. *et al.* The muscle-specific microRNA miR-206 blocks human rhabdomyosarcoma growth in xenotransplanted mice by promoting myogenic differentiation. *J. Clin. Invest.* **119,** 2366–2378 (2009).
51. Zhou, Y. *et al.* Chimeric mouse tumor models reveal differences in pathway activation between ERBB family- and KRAS-dependent lung adenocarcinomas. *Nat. Biotechnol.* **28,** 71–78 (2010).
52. Harada, R. *et al.* Genome-wide location analysis and expression studies reveal a role for p110 CUX1 in the activation of DNA replication genes. *Nucleic Acids Res.* **36,** 189–202 (2008).
53. Szulc, J., Wiznerowicz, M., Sauvain, M. O., Trono, D. & Aebischer, P. A versatile tool for conditional gene expression and knockdown. *Nat. Methods* **3,** 109–116 (2006).
54. Maeda, S. *et al.* Ikappa B kinasebeta/nuclear factor-kappaB activation controls the development of liver metastasis by way of interleukin-6 expression. *Hepatology* **50,** 1851–1860 (2009).
55. Elmén, J. *et al.* LNA-mediated microRNA silencing in non-human primates. *Nature* **452,** 896–899 (2008).
56. Bai, S. *et al.* MicroRNA-122 inhibits tumorigenic properties of hepatocellular carcinoma cells and sensitizes these cells to sorafenib. *J. Biol. Chem.* **284,** 32015–32027 (2009).
57. Yao, X. *et al.* A novel orthotopic tumor model to study growth factors and oncogenes in hepatocarcinogenesis. *Clin. Cancer Res.* **9,** 2719–2726 (2003).
58. Kim, M. *et al.* Generation of orthotopic and heterotopic human pancreatic cancer xenografts in immunodeficient mice. *Nat. Protoc.* **4,** 1670–1680 (2009).

Acknowledgments

This work was supported by Grants-in-Aid from the Ministry of Education, Culture, Sports, Science and Technology, Japan (#22390058, #22590718, #17016016 and #20390204) (to M. Otsuka, Y. Kondo, M. Omata and K. Koike), by Health Sciences Research Grants of The Ministry of Health, Labour and Welfare of Japan (Research on Hepatitis) (to K. Koike), by grants from the Takeda Science Foundation, Astellas Foundation for Research on Metabolic Disorders, Senri Life Science Foundation, the Foundation for Promotion of Cancer Research and the Mochida Memorial Foundation for Medical and Pharmaceutical Research (to M. Otsuka), and by the grant 019389 from the Canadian Cancer Society (to A.N.).

Author contributions

K. Kojima, M. Otsuka and A.N. planned the research and wrote the paper. K. Kojima, A.T., C.V., T.Y., Y. Kondo, Y. Kang and Z.X. performed the majority of the experiments. M.A., N.K., W.Z. and A.N. contributed materials. T.K. and H.Y. supported several experiments. M. Omata and K. Koike supervised the entire project.

Additional information

Supplementary Information accompanies this paper at http://www.nature.com/naturecommunications

Competing financial interests: The authors declare no competing financial interests.

Reprints and permission information is available online at http://npg.nature.com/reprintsandpermissions/

How to cite this article: Kojima, K. *et al.* MiRNA122 is a key regulator of α-fetoprotein expression and influences the aggressiveness of hepatocellular carcinoma. *Nat. Commun.* 2:338 doi: 10.1038/ncomms1345 (2011).

Liver INTERNATIONAL
OFFICIAL JOURNAL OF THE INTERNATIONAL ASSOCIATION FOR THE STUDY OF THE LIVER

Liver International ISSN 1478-3223

CLINICAL STUDIES

Intrahepatic bile duct dilatation after percutaneous radiofrequency ablation for hepatocellular carcinoma: impact on patient's prognosis

Yuji Kondo, Shuichiro Shiina, Ryosuke Tateishi, Toru Arano, Koji Uchino, Kennichiro Enooku, Eriko Goto, Hayato Nakagawa, Ryota Masuzaki, Yoshinari Asaoka, Hajime Fujie, Tadashi Goto, Masao Omata, Haruhiko Yoshida and Kazuhiko Koike

Department of Gastroenterology, Graduate School of Medicine, The University of Tokyo, Tokyo, Japan

Keywords
bile duct dilatation – hepatocellular carcinoma – radiofrequency ablation

Abbreviations
AFP, α-fetoprotein; CT, computed tomography; DCP, des-γ-carboxy prothrombin; HCC, hepatocellular carcinoma; MRI, magnetic resonance imaging; RFA, radiofrequency ablation.

Correspondence
Yuji Kondo, Department of Gastroenterology, Graduate School of Medicine, The University of Tokyo, Tokyo, Japan
Tel: +81 3 3815 5411
Fax: +81 3 3814 0021
e-mail: ykon-tky@umin.ac.jp

Received 9 October 2010
Accepted 7 November 2010

DOI:10.1111/j.1478-3231.2010.02415.x

Abstract

Background: Percutaneous radiofrequency ablation (RFA) has been widely accepted as an alternative to surgery for small hepatocellular carcinoma (HCC). In RFA, a portion of liver tissue surrounding tumour is also ablated to achieve a safety margin. The intrahepatic bile duct may be injured and result in chronic bile duct dilatation upstream of the injured site. However, the impact of such an injury on the overall prognosis has been unclear. *Methods:* Patients who showed bile duct dilatation following RFA were identified by a retrospective review of imaging studies. Each dilatation was classified as mild (limited to one hepatic subsegment) or severe (affecting two or more subsegments). The relation between the incidence of intrahepatic bile duct dilatation and HCC recurrence or survival was analysed using proportional hazard models. *Results:* Among 589 consecutive HCC patients treated with RFA, 70 (11.9%) and 21 (3.6%) patients showed mild and severe bile duct dilatation respectively. Patients with severe dilatation, but not those with mild dilatation, had lower survival and higher HCC recurrence than patients without dilatation. Severe dilatation, but not mild dilatation, was significantly associated with death [hazard ratio (HR) 2.17, $P = 0.035$] and recurrence (HR 2.89, $P < 0.001$). *Conclusion:* Whereas mild bile duct dilatation after RFA is clinically negligible, bile duct dilatation affecting two or more subsegments should be regarded as a complication that may affect the prognosis and should be observed carefully.

Hepatocellular carcinoma (HCC) is one of the most common cancers worldwide (1, 2). Apart from liver transplantation, surgical resection is the optimal treatment of choice for HCC. However, the majority of HCC patients have background chronic liver diseases, especially cirrhosis, and a substantial proportion of patients are not eligible for surgical resection because of impaired liver function and/or multinodularity of the tumour. In such patients, less invasive percutaneous tumour ablation procedures have been applied, such as ethanol injection, microwave coagulation and radiofrequency ablation (RFA) (3, 4). Among them, RFA is currently the most widely accepted alternative to surgery because of its safety and high efficacy (5, 6).

The RFA applies thermal energy converted from radiofrequency current to the coagulation of tumour tissues. However, the thermal energy may also affect intra- and extrahepatic tissues, resulting in complications specific to RFA (7). We have characterized haemorrhagic complications following RFA (8), such as haemoperitoneum and haemothorax, and reported techniques such as intraperitoneal fluid infusion to prevent extrahepatic thermal injuries (9). Intrahepatic bile duct dilatation may appear several months after RFA. The dilatation is thought to represent downstream bile duct stricture caused by RFA-related thermal injuries. Thus, intrahepatic bile duct dilatation, or thermal injury to intrahepatic bile ducts, is another complication specific to RFA, which has not been well characterized.

In RFA, thermal energy is generated concentrical to the electrode and inevitably affects the surrounding liver parenchyma. In fact, we usually ablate a portion of surrounding liver intentionally to achieve sufficient safety margin. Blood vessels are thought to be relatively immune to the thermal injury because of the cooling effect of circulating fluid. On the other hand, the velocity of bile juice in the bile duct is much slower, and intrahepatic bile ducts near the tumour are prone to thermal injury during RFA. However, the injury to bile ducts cannot be recognized until some macroscopic changes, such as bile duct dilatation upstream of stenosis because of thermal injury, become visible on imaging

studies. Minimal injuries without visible ductal dilatation cannot be recognized, and such injuries seem to have little clinical significance. Recognizable bile duct dilatation that appears after RFA is not rare, reported to be found in 17% of patients (10). However, its impact on patient's prognosis remains unknown. In the current study, we sought to evaluate the effects of thermal injuries to intrahepatic bile ducts by comparing the survival rate and the HCC recurrence rate between patients with and without visible bile duct dilatation after RFA.

Patients and methods

Patients

Between January 2003 and December 2007, a total of 589 patients with HCC received RFA as the initial treatment at the Department of Gastroenterology, University of Tokyo Hospital. All patients were prospectively registered on an electronic database, and the current study was based on data observed until the end of December 2008. The flowchart of the current study is presented in Figure 1. Each patient underwent contrast-enhanced computed tomography (CT) or magnetic resonance imaging (MRI) about every 4 months after RFA for the screening of HCC recurrence. In the current study, those imaging studies were reviewed retrospectively to identify intrahepatic bile duct dilatation after RFA. We placed no restriction on RFA solely by the location of tumours (11). Thus, tumours adjacent to an intrahepatic bile duct, possibly at a high risk for bile duct injury, were also treated with RFA, if other conditions met the indication criteria for RFA, as described below.

Hepatocellular carcinoma was diagnosed mainly based on the typical findings on diagnostic imaging, i.e., hyperattenuation in the arterial phase and hypo-attenuation in the portal-venous phase on contrast-enhanced dynamic CT or MRI (12). Percutaneous needle biopsy was reserved for tumours not typical on imaging studies.

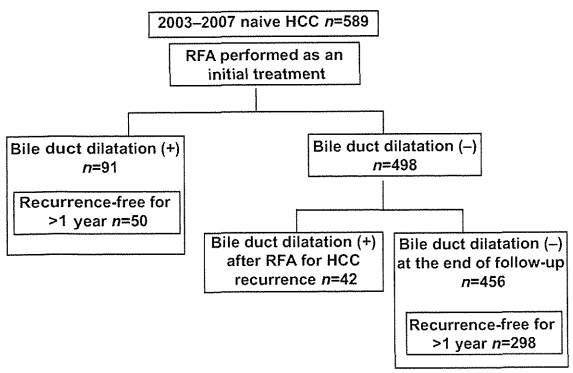

Fig. 1. Schematic flowchart of the study. HCC, hepatocellular carcinoma; RFA, radiofrequency ablation.

Radiofrequency ablation

The inclusion criteria for RFA in the author's institution were as follows: tumour size not larger than 3 cm in diameter, tumour number not more than three, absence of vascular invasion or extrahepatic metastasis, serum total bilirubin concentration not higher than 3 mg/dl, platelet count no less than $50 \times 10^3/mm^3$, prothrombin activity no less than 50% (approximately 1.5 INR) and absence of uncontrollable ascites. Patients with a prior history of bilioenteric anastomosis or sphincterotomy were excluded because these conditions were risk factors for hepatic abscess formation after RFA. RFA was sometimes performed on patients with a tumour size larger than 3 cm or tumour number more than three, when RFA could be expected to improve survival after careful consideration. A written informed consent was obtained from each patient, and family members when appropriate, before RFA.

The RFA was performed on an in-patient basis. The details of the RFA procedure have been described elsewhere (13). In summary, RFA was performed with a 17 G internally cooled electrode system (Valleylab, Boulder, CO, USA) (14, 15) with a 2 or 3 cm exposed tip, which was inserted under real-time ultrasound guidance. Intrapleural or intraperitoneal fluid infusion was performed before electrode needle insertion, if appropriate, according to the previous reports (9, 16). RFA was started at 60 and 40 W for the 3 and 2 cm exposed tips, respectively, and the power was increased in a stepwise fashion by 20 W/min. The duration of a single ablation was 12 min for the 3 cm electrode and 6 min for the 2 cm electrode.

Dynamic CT was performed within 3 days after treatment. Complete tumour necrosis was defined as hypo-attenuation of the entire lesion with a sufficient surrounding margin. Patients received additional RFA until complete necrosis was confirmed. After complete tumour ablation, patients were followed up at the outpatient clinic every 4 months with enhanced three-phase dynamic CT or MRI. In the current study, all these CT images performed in the follow-up period were reviewed for the presence of any intrahepatic bile duct dilatation. Patients who had HCC recurrence were treated with RFA again or transcatheter arterial chemoembolization appropriately according to the tumour size and number, liver function reserve and general medical conditions.

Definition of bile duct dilatation

Bile duct injury can be recognized only as an upstream distal bile duct dilatation on imaging studies. In the current study, any disproportional dilatation of intrahepatic bile ducts, including biloma, in the upstream of the ablated area that was newly detected on dynamic enhanced CT or MRI after RFA was defined as a bile duct injury because of RFA. This definition was in accordance with the previous study by Kim *et al.* (10). Dilatation of a bile duct that had existed before the initial RFA, or that

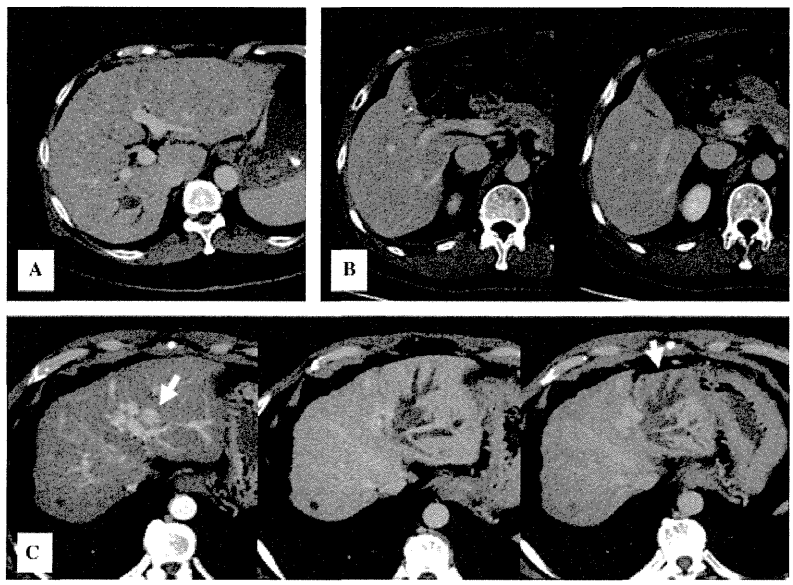

Fig. 2. Typical cases with bile duct dilatation after radiofrequency ablation (RFA); (A) 63-year-old male with peripheral bile duct dilatation after RFA for hepatocellular carcinoma (HCC) in Segment 7; (B) 67-year-old male with subsegmental bile duct dilatation after RFA for hepatocellular carcinoma in Segment 5. (C) 49-year-old male with segmental bile duct dilatation. Left: HCC located adjacent to the Glisson's capsule, 2.2 cm in diameter, was detected (arrow) in a patient with cirrhosis because of hepatitis C infection. Middle: intrahepatic bile ducts (B2 and B3) were markedly dilated 4 months after RFA. Right: atrophy of hepatic parenchyma in the lateral segment was noted 1 year after RFA (arrow), without any recurrence of HCC.

was because of other mechanical process, such as biliary invasion of HCC, was not considered as an event of bile duct dilatation in the current study.

The bile duct dilatations found in the current study were divided into two categories, mild or severe, according to the distribution of dilated bile ducts. Mild dilatation was defined as dilatation limited to one hepatic subsegment, whereas severe dilatation was defined as dilatation in two or more subsegments. Some typical cases are presented in Figure 2. The extent of bile duct dilatation was judged on the last CT/MRI performed in the follow-up period.

Statistical analyses

Comparisons of the two groups were performed with Student's *t*-test for continuous variables and Fisher's exact test for frequency distributions. The survival curves were created with the Kaplan–Meier method. Two survival curves were compared with log-rank test. A *P*-value < 0.05 on a two-tailed test was considered statistically significant. To predict death and recurrence after RFA, a proportional hazard model was used, which included the severity of bile duct dilatation, age, gender, hepatitis C virus, Child–Pugh classification of liver function, maximum tumour size, tumour number, α-fetoprotein (AFP) and des-γ-carboxy prothrombin (DCP) as independent variables in univariate analyses. Severity of bile duct dilatation was treated as a trichotomous variable (none, mild or severe) and analysed using two dummy variables. In multivariate analyses, the two dummy variables were included together with variables with *P*-value < 0.05 in univariate analyses. All statistical analyses were performed using JMP 8 (SAS institute Japan, Tokyo, Japan) software.

Results

Patient characteristics

Of 589 patients, bile duct dilatation because of the initial RFA developed in 91 (15%) patients during the observation period. There were 70 patients with mild dilatation (limited to one subsegment; incidence among all patients, 11.9%) and 21 patients with severe dilatation (affecting two or more subsegments; 3.6%). There were 42 (7.1%) additional patients with bile duct dilatation that was detected after RFA for recurrent HCC, which we assumed to be because of the latter RFA. These 42 patients were excluded from the survival analyses because the impacts on the prognosis of the bile duct injury and HCC recurrence were indistinctive in these patients, whereas in analyses of recurrence after initial RFA, they were included in the control (without bile duct injury) group because bile duct dilatation was not related to the first recurrence in these patients. The remaining 456 patients had not developed any bile duct dilatation until the end of follow-up. The interval between the initial RFA and the detection of bile duct dilatation was shorter than 6 months in 70 (77%), 6–12 months in 13 (14%),

Table 1. Baseline characteristics of patients with or without bile duct injury

		After initial RFA ($n=91$)					
Bile duct dilatation	Absent ($n=456$)	Mild ($n=70$)	*P*	Severe ($n=21$)	*P*	After RFA for recurrence ($n=42$)	*P*
Mean age (year)	68.4 (8.43)	69.2 (8.08)	0.44	68.7 (10.24)	0.90	69.0 (7.61)	0.64
Age (< 70/≥70)	252/204	38/32	0.90	11/10	0.83	23/19	1.00
Gender (male/female)	295/161	42/28	0.50	16/5	0.35	24/18	0.40
HCV (positive/negative)	346/110	48/22	0.24	16/5	1.00	35/7	0.34
Child–Pugh grade (A/BC)	334/122	46/24	0.20	16/5	0.81	28/14	0.37
Tumour size (< 2cm/≥2cm)	189/267	23/47	0.19	6/15	0.27	13/29	0.19
Tumour diameter (cm)	2.45 (10.15)	2.42 (7.58)	0.78	2.79 (11.34)	0.14	2.31 (6.03)	0.43
Tumour number (= < 2/≥3)	362/94	55/15	1.00	15/6	0.41	32/10	0.69
Mean tumour number	1.78 (1.16)	1.87 (1.26)	0.53	2.33 (1.96)	0.04	1.69 (1.02)	0.57
AFP (< /≥100 (ng/ml)	370/86	51/19	0.11	16/5	0.78	33/9	0.84
DCP (< /≥100 (mAU/ml)	385/71	53/17	0.08	16/5	0.36	38/5	0.52

Continuous variables are presented as mean (SD).

AFP, α-fetoprotein; DCP, des-γ-carboxy prothrombin; HCV, hepatitis C virus; RFA, radiofrequency ablation.

1–2 years in 6 (7%) and beyond 2 years in two (2%) patients. Bile duct dilatation was found in the left lobe in 43, the right lobe in 45 and was bilobular in three patients.

The characteristics of the included patients immediately before the initial RFA are presented in Table 1. Most characteristics did not differ significantly between patients who subsequently presented bile duct dilatation and those who did not. However, the mean number of tumours was significantly greater in patients with severe bile duct dilatation than in those without dilatation (2.33 vs. 1.78, $P=0.04$).

The details of the 21 patients with severe bile duct dilatation are presented in Table 2. In 19 of them, the tumour was adjacent to a major portal venous branch, namely, the umbilical portion of the left portal branch, the right anterior branch or the right posterior branch. Because portal veins and intrahepatic bile ducts run parallel in the liver, we can assume that these tumours were also adjacent to the corresponding bile ducts. The remaining two patients had a tumour adjacent to two subsegmental branches. HCC recurrence after curative ablation was identified in 18 patients, two with local tumour progression, 15 with intrahepatic recurrence distant from the primary tumour and the remaining one with extrahepatic metastasis.

To assess the relationship between tumour location and the incidence of severe bile duct dilatation, 302 patients with uninodular HCC were analysed. The incidence of severe bile duct dilatation was 0% (0/5), 6.5% (3/46), 0% (0/35), 0.7% (1/143) and 4.1% (3/73) in patients with a tumour located in the caudate lobe (Segment 1), the left lateral segment, the left medial segment, the right anterior segment and the right posterior segment respectively. Although statistical analysis was not applicable because of the small number of patients with severe bile duct dilatation, tumours located in the left lateral or the right posterior segment seemed to be at a higher risk of developing severe bile duct dilatation after RFA.

Impact of bile duct dilatation on liver function

To assess the impact of bile duct dilatation after RFA on liver function reserve, changes in serum albumin and the total bilirubin concentrations 6 months and 1 year after RFA were calculated. Those patients who had HCC recurrence within 1 year after the ablation were excluded from this analysis of liver function changes because HCC recurrence and its treatment may have affected liver function and obscured the impact of bile duct dilatation induced by the initial RFA. HCC recurrence occurred within 1 year after the initial RFA in 158 of 456 patients without bile duct dilatation, 30 of 70 patients with mild dilatation and 11 of 21 patients with severe dilatation. Thus, 50 patients with bile duct dilatation (40 with mild dilatation and 10 with severe dilatation) and 298 patients without were analysed. No patients died without HCC recurrence within 1 year after the initial RFA. The baseline characteristics did not differ between the patients with mild or severe bile duct dilatation and those without (data not shown), except that DCP > 100 was more frequent in patients with mild dilatation than in patients without bile duct dilatation ($P=0.03$).

The changes in the serum albumin concentration in the three groups (patients without dilatation, patients with mild dilatation and patients with severe dilatation) are presented in Table 3. The baseline value and the decrease in 6 months were not different among the three groups. However, the decrease in 1 year was significantly greater in patients with mild or severe dilatation. The changes in the serum total bilirubin concentration are presented in Table 3. The baseline value was greater in patients with mild dilatation than that in patients without dilatation. The increase in the total bilirubin concentration in 6 months was significantly greater in the

Table 2. The 21 patients with severe bile duct dilatation

Patients	Age	Gender	Maximum tumour diameter (mm)	Tumour number	Tumour location*	Adjacent portal venous branches†	Affected subsegments	Recurrence‡	Time to recurrence (year)	Type of first recurrence§	Observation period (year)	outcome	Cause of death‖
1	65	M	40	2	8	A	5, 6, 7, 8	+	0.9	Distant	5.4	Dead	HF
2	69	M	22	1	3	U	2, 3	+	1.3	Local	5.5	Censored	
3	66	F	24	2	3	U	2, 3	+	0.7	Distant	4.9	Dead	HCC
4	66	M	22	3	7	P	5, 7, 8	+	0.8	Distant	4.1	Censored	
5	77	M	51	10	2	U	2, 3	NA	–	–	2.5	Dead	HCC
6	64	M	18	2	2	U	2, 3	+	0.6	Extrahepatic	4.6	Dead	HCC
7	64	M	16	2	5	A, P	5, 6, 7, 8	+	1.4	Distant	3.9	Dead	HCC
8	79	M	29	3	4, 8	4, A, 6	4, 5, 6, 8	+	0.4	Distant	3.4	Dead	HCC
9	57	F	26	2	4	U	2, 3, 4	+	2.4	Distant	3.7	Censored	
10	78	M	21	6	2	U	2, 3	NA	–	–	1.2	Dead	HF
11	79	F	40	2	4	U	2, 3	+	0.3	Distant	1.1	Dead	HF
12	76	M	18	2	8	A, P	5, 8	+	0.5	Distant	2.9	Censored	
13	84	M	50	1	6	P	6, 7	+	0.4	Local	1.2	Dead	HCC
14	72	F	19	2	5	5	5, 8	+	1.2	Distant	2.9	Censored	
15	73	M	16	1	2	U	2, 4	+	1.2	Distant	2.5	Censored	
16	79	F	24	3	8	5, 8	5, 8	+	0.8	Distant	2.5	Censored	
17	57	M	18	3	2, 5	U, A	2, 5	+	0.9	Distant	1.4	Dead	HF
18	76	M	41	1	7	P	6, 7	+	0.9	Distant	1.8	Censored	
19	46	M	27	1	7	P	6, 7	+	1.0	Distant	1.1	Censored	
20	49	M	21	1	3	U	2, 3	+	1.6	Distant	1.7	Censored	
21	65	M	43	1	8	A	5, 8	–	–	–	1.3	Censored	

*The subsegment in which the tumour responsible for severe bile duct dilatation was mainly located.

†Portal venous branches to which the tumour was adjacent on CT or MRI were presented. U, umbilical portion of the left portal vein; A, right anterior branch; P, right posterior branch.

‡Patients 5 and 10 were treated without a curative intent because of tumour multiplicity. +, present; –, absent; NA, not applicable.

§Distant, intrahepatic recurrence distant from the primary tumour(s); local, local tumour progression; extrahepatic, extrahepatic tumour metastasis.

‖CT, computed tomography; HCC; hepatocellular carcinoma progression; HF, hepatic failure; MRI, magnetic resonance imaging.

Table 3. Change of serum albumin and the total bilirubin concentration in 6 months and 1 year after the initial radiofrequency ablation in patients without any recurrence for at least 1 year

Bile duct dilatation	Absent ($n = 298$)	Mild ($n = 40$)	P	Severe ($n = 10$)	P
Albumin (g/dl)					
Value before RFA	3.71 (0.44)	3.72 (0.46)	0.88	3.70 (0.45)	0.90
Change in 6 months	−0.03 (0.28)	−0.04 (0.23)	0.86	−0.02 (0.23)	0.95
Change in 1 year	−0.06 (0.31)	−0.35 (0.96)	< 0.01	−0.25 (0.31)	0.01
Total bilirubin (mg/dl)					
Value before RFA	0.88 (0.44)	1.14 (0.72)	< 0.01	1.00 (0.82)	0.41
Change in 6 months	+0.13 (0.31)	+0.31 (0.71)	< 0.01	+0.13 (0.16)	0.67
Change in 1 year	+0.18 (0.58)	+0.15 (0.35)	0.80	+0.28 (0.26)	0.27

Data are presented as mean (SD).

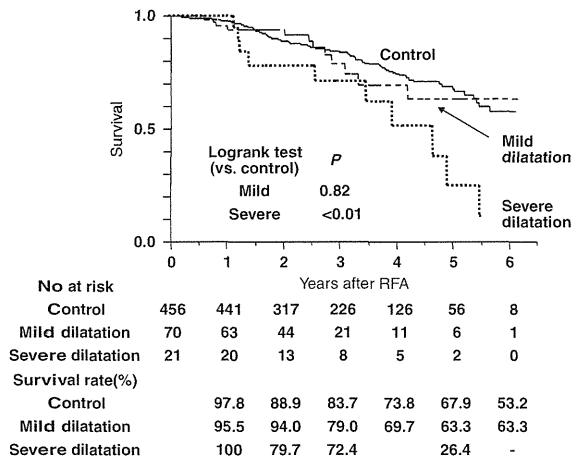

Fig. 3. Cumulative survival of patients with mild and severe bile duct dilatation compared with those without bile duct dilatation. RFA, radiofrequency ablation.

patients with mild dilatation than in those without dilatation. However, the increase was not different between patients with severe dilatation and patients without dilatation, and the increase in 1 year was not different among the three groups.

Survival after radiofrequency ablation in patients with and without bile duct dilatation

The overall survival was compared between patients with and without bile duct dilatation, excluding those who showed dilatation only after RFA for HCC recurrence ($n = 42$). The survival curves created with Kaplan–Meier method are presented in Figure 3. The survival of patients with mild bile duct dilatation was not significantly different from that of patients without bile duct dilatation (control group). However, the survival of patients with severe bile duct dilatation was significantly lower ($P < 0.001$ by the log-rank test) than that of the control group. Ten out of 21 patients with severe bile duct dilatation died during the study period. The cause of death was hepatic failure in spite of controlled HCC in four and HCC progression in six patients.

The results of univariate and multivariate analyses to predict death based on proportional hazard model are presented in Table 4. In the univariate analysis, severe bile duct dilatation, age (older than 70), Child–Pugh classification (B or C), tumour number (more than three), AFP (> 100ng/ml) and DCP (> 100 mAu/ml) before RFA were selected as potential predictors of death. In the multivariate analysis, mild bile duct dilatation vs. no dilation, severe dilatation vs. no dilatation, together with other clinical factors, were used as independent variables. Although mild bile duct dilatation was not significant [hazard ratio (HR) 1.01, $P = 0.973$], severe bile duct dilatation was one of the significant predictors of death (HR 2.17, $P = 0.035$). In addition to severe bile duct dilatation, hepatitis C virus positivity, Child–Pugh classification (B/C vs. A) and tumour number (≥ 3) were significant predictors of death.

Hepatocellular carcinoma recurrence after radiofrequency ablation in patients with and without bile duct dilatation

In the analysis of HCC recurrence, patients with bile duct dilatation after RFA for recurrence, who were excluded from the survival above analyses, were combined with patients without bile duct dilatation (control). Patients treated by RFA without a curative intent were excluded (one from the mild dilatation group, two from the severe dilatation group and 13 from the control group), and thus 69 patients with mild bile duct dilatation, 19 with severe dilatation and 485 without dilatation (control) were analysed. Patients who died without HCC recurrence (two in the mild dilatation group, two in the severe dilatation group and 31 in the control group) were treated as censored.

The curves of cumulative HCC recurrence created with the Kaplan–Meier method are presented in Figure 4. The cumulative recurrence did not differ significantly between patients with mild bile duct dilatation and the controls, whereas patients with severe dilatation showed significantly higher cumulative recurrence than the controls ($P < 0.001$). During the study period, all 19 patients

Table 4. Univariate and multivariate analyses to predict death using the Cox proportional hazard model

	Univariate analysis			Multivariate analysis		
Variables at the initial RFA	HR	95% CI	*P*	HR	95% CI	*P*
Bile duct dilatation						
None	1			1		
Mild	1.04	0.54–1.82	0.889	1.01	0.52–1.77	0.973
Severe	2.45	1.20–4.46	0.017	2.17	1.06–3.96	0.035
Age (year) > 70	1.43	1.00–2.04	0.050			
Gender, male	1.24	0.85–1.85	0.261			
Hepatitis C virus (+)	1.56	1.01–2.51	0.045	1.60	1.62–3.34	0.040
Child–Pugh classification, B or C	2.63	1.83–3.74	< 0.001	2.33	1.62–3.34	< 0.001
Maximum tumour size > 2.0cm	1.33	0.93–1.95	0.122			
Tumour number ≥3	2.27	1.55–3.28	< 0.001	1.95	1.32–2.84	< 0.001
AFP (ng/ml) ≥100	1.62	1.06–2.38	0.024	1.44	0.94–2.15	0.090
DCP (mAu/ml) ≥100	1.77	1.13–2.67	0.013	1.63	1.03–2.50	0.037

AFP, α-fetoprotein; CI, confidence interval; DCP, des-γ-carboxy prothrombin; HR, hazard ratio; RFA, radiofrequency ablation.

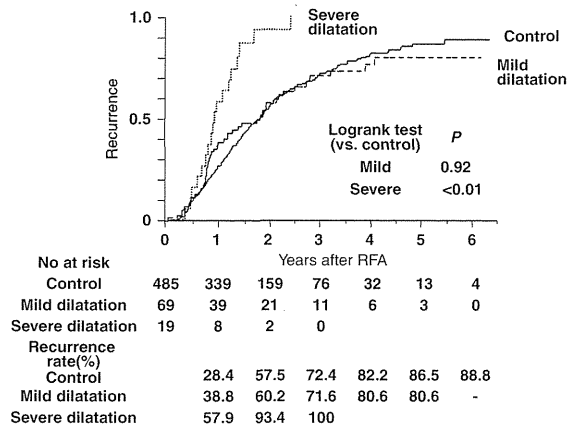

Fig. 4. HCC recurrence rates in patients with mild and severe bile duct dilatation compared with those without bile duct dilatation. HCC, hepatocellular carcinoma; RFA, radiofrequency ablation.

with severe bile duct dilatation developed HCC recurrence, local tumour progression in one, recurrence in the same subsegment as the bile duct dilatation in four, the same segment in two, other segments in 10, portal vein invasion in one and extrahepatic metastasis in one patient.

The results of univariate and multivariate analyses using the proportional hazard model are presented in Table 5. In the univariate analysis, severe bile duct dilatation, hepatitis C virus positivity, Child–Pugh classification (B or C), maximum tumour size (> 2.0 cm), tumour number (more than three), AFP (> 100 ng/ml) and DCP (> 100 mAu/ml) before RFA were selected as potential predictors of recurrence. Multivariate analysis was performed as in the analysis of overall survival shown above. Mild bile duct dilatation was not a significant predictor of recurrence (HR 1.01, $P = 0.959$), whereas severe bile duct dilatation was significant (HR 2.89, $P < 0.001$). Other significant predictors of recurrence were hepatitis C virus positivity, Child–Pugh classification (B or C), maximum tumour size (> 2.0 cm), tumour number (more than three), AFP (> 100 ng/ml) and DCP (> 100 mAu/ml).

Discussion

In the current study with a long-term follow-up, bile duct dilatation was found in 15% of patients who underwent RFA for HCC. However, most cases of bile duct dilatation were limited to a single subsegment of the liver, and we did not find a significant influence of such dilatation on the overall survival or HCC recurrence. However, severe bile duct dilatation, defined as dilatation in two or more subsegments, developed in 21/589 (3.6%) patients and this was shown to be associated with poorer survival and a higher incidence of HCC recurrence. Thus, severe bile duct dilatation should be regarded as a long-term complication of RFA, and patients who developed severe bile duct dilatation should be followed carefully. However, because the incidence of severe bile duct dilatation was acceptably low, the indication of RFA should not be restricted solely for fear of bile duct injury, at least in highly experienced institutions.

The liver function was slightly but significantly deteriorated in HCC recurrence-free patients with bile duct dilatation after RFA, although this patient selection may lead to underestimation of the deterioration of liver function. The decrease in the serum albumin concentration in 1 year, but not in the first 6 months, following RFA was significantly greater in patients with than in patients without bile duct dilatation. Patients with bile duct dilatation seem to show slow progressive impairment in hepatic function and the deterioration of liver function in the longer term may be more severe. In the current study, four of 10 patients with severe bile duct dilatation died of hepatic failure while HCC was well controlled. Admittedly, in order to elucidate the

Table 5. Univariate and multivariate analyses to predict recurrence using the Cox proportional hazard model

	Univariate analysis			Multivariate analysis		
Variables at initial RFA	HR	95% CI	*P*	HR	95% CI	*P*
Bile duct dilatation						
None	1			1		
Mild	1.09	0.78–1.47	0.603	1.01	0.72–1.37	0.959
Severe	2.94	1.75–4.63	< 0.001	2.89	1.72–4.55	< 0.001
Age (year) > 70	0.98	0.80–1.19	0.814			
Gender, male	0.97	0.80–1.20	0.800			
Hepatitis C virus (+)	1.31	1.04–1.67	0.023	1.41	1.10–1.82	0.007
Child–Pugh classification, B or C	1.38	1.10–1.71	0.005	1.36	1.07–1.72	0.013
Maximum tumour size > 2.0cm	1.29	1.06–1.58	0.012	1.23	0.98–1.54	0.07
Tumour number ≥3	1.73	1.37–2.17	< 0.001	1.63	1.26–2.08	< 0.001
AFP (ng/ml) ≥100	1.42	1.11–1.79	0.005	1.43	1.10–1.84	0.009
DCP (mAu/ml) ≥100	1.65	1.27–2.12	< 0.001	1.60	1.20–2.10	0.002

AFP, α-fetoprotein; CI, confidence interval; DCP, des-γ-carboxy prothrombin; HR, hazard ratio; RFA, radiofrequency ablation.

mechanism by which liver function deteriorates in patients with severe bile duct dilatation, the current study was limited by the small number of such patients. However, exacerbated liver dysfunction in the liver parenchyma upstream of bile duct stricture because of cholestasis may be a likely possibility.

In this series, four patients (Patient 1, 10, 11 and 17 in Table 2) died of hepatic failure although HCC was well controlled. Not surprisingly, patients with impaired liver function before RFA seem to be prone to hepatic failure because of severe bile duct dilatation. In fact, patients 10 and 17 had moderate cirrhosis, and the bile duct injury seemed to accelerate liver dysfunction. Patient 11 had aggressive HCC in severe cirrhotic liver, which required repeated RFA and transcatheter arterial chemoembolization. She died of hepatic failure probably because of treatment-related liver damage. On the other hand, Patient 1 had good liver function reserve before the initial RFA. He developed frequent HCC recurrence and RFA was repeated. Continuous percutaneous bile duct drainage was required for jaundice 3 years after the initial RFA, and he died of hepatic failure at 5.4 years. In patients who already have had severe bile duct dilatation, impairment of hepatic function by the treatment procedure for HCC recurrence was more severe, especially when the procedure was repeated. Therefore, treatment for recurrence should be planned carefully in such patients.

In the current study, severe bile duct dilatation was also found to be associated with a higher incidence rate of HCC recurrence, which may have worsened the prognosis of such patients. Six of 10 patients with severe bile duct dilatation died of HCC progression. The reason for this association between severe dilatation and a higher recurrence rate is unclear. It may be postulated that tumours adjacent to major intrahepatic bile ducts may be prone to receive insufficient ablation and consequently the recurrence rate is high. However, in the current study, only two patients developed local tumour progression among the 19 radically treated patients complicated with severe bile duct injury. Another possible explanation is that tumours associated with bile duct injury on RFA are more likely to have an invasive nature, namely, microscopic invasion into Glisson's capsule, portal vein or bile duct, which may have been accompanied by undetectable intrahepatic or extrahepatic metastases at the time of RFA.

Therefore, the worse prognosis of the patients with severe dilatation may be attributed not only to deterioration of liver function because of bile duct injury itself but also a higher rate of HCC recurrence. Considering that HCC progression and hepatic failure (in spite of controlled HCC) were found approximately equally to be patients' cause of death, these two factors had a similar impact on the prognosis of these patients.

Two distinct procedures have been reported for the prevention of bile duct injury by RFA, namely, prophylactic biliary stent placement and intraductal cooling of biliary duct with chilled saline during RFA (17–20), neither of which were used in the current study. These techniques require an endoscopic transpapillary insertion of a biliary drainage tube or laparotomy, which can be complicated by bleeding, pancreatitis or cholangitis. Such an invasive and complex nature may preclude further acceptance of these procedures as a routine for the prevention of bile duct injury, considering particularly the low incidence of severe bile duct dilatation. At present, the indication of such procedures should be carefully considered in each individual case. For tumours with an extremely high risk of developing severe bile duct dilatation after RFA, a percutaneous ethanol injection may be a safer alternative, although it may require more treatment sessions and higher technical expertise to ensure complete necrosis of the tumour (5, 21).

In conclusion, mild bile duct dilatations after RFA are clinically negligible and need not be regarded as a complication. However, bile duct dilatations affecting two or more hepatic subsegments should be regarded as a major complication of RFA, which may be associated with a poorer prognosis and should be observed carefully.

Acknowledgements

The authors have no conflict of interest to disclose.

References

1. El-Serag HB, Mason AC. Rising incidence of hepatocellular carcinoma in the united states. *N Engl J Med* 1999; **340**: 745–50.
2. Colombo M. Screening and diagnosis of hepatocellular carcinoma. *Liver Int* 2009; **29**(Suppl. 1): 143–7.
3. Omata M, Tateishi R, Yoshida H, Shiina S. Treatment of hepatocellular carcinoma by percutaneous tumor ablation methods: ethanol injection therapy and radiofrequency ablation. *Gastroenterology* 2004; **127**(Suppl. 1): S159–66.
4. Shiina S, Teratani T, Obi S, *et al.* Nonsurgical treatment of hepatocellular carcinoma: from percutaneous ethanol injection therapy and percutaneous microwave coagulation therapy to radiofrequency ablation. *Oncology* 2002; **62**(Suppl. 1): 64–8.
5. Shiina S, Teratani T, Obi S, *et al.* A randomized controlled trial of radiofrequency ablation with ethanol injection for small hepatocellular carcinoma. *Gastroenterology* 2005; **129**: 122–30.
6. Lin SM, Lin CJ, Lin CC, *et al.* Radiofrequency ablation improves prognosis compared with ethanol injection for hepatocellular carcinoma < or = 4 cm. *Gastroenterology* 2004; **127**: 1714–23.
7. Mulier S, Mulier P, Ni Y, *et al.* Complications of radiofrequency coagulation of liver tumours. *Br J Surg* 2002; **89**: 1206–22.
8. Goto E, Tateishi R, Shiina S, *et al.* Hemorrhagic complications of percutaneous radiofrequency ablation for liver tumors. *J Clin Gastroenterol* 2010; **44**: 374–80
9. Kondo Y, Yoshida H, Shiina S, *et al.* Artificial ascites technique for percutaneous radiofrequency ablation of liver cancer adjacent to the gastrointestinal tract. *Br J Surg* 2006; **93**: 1277–82.
10. Kim SH, Lim HK, Choi D, *et al.* Changes in bile ducts after radiofrequency ablation of hepatocellular carcinoma: frequency and clinical significance. *Am J Roentgenol* 2004; **183**: 1611–7.
11. Teratani T, Yoshida H, Shiina S, *et al.* Radiofrequency ablation for hepatocellular carcinoma in so-called high-risk locations. *Hepatology* 2006; **43**: 1101–8.
12. Torzilli G, Minagawa M, Takayama T, *et al.* Accurate preoperative evaluation of liver mass lesions without fine-needle biopsy. *Hepatology* 1999; **30**: 889–93.
13. Tateishi R, Shiina S, Teratani T, *et al.* Percutaneous radiofrequency ablation for hepatocellular carcinoma. An analysis of 1000 cases. *Cancer* 2005; **103**: 1201–9.
14. Lorentzen T. A cooled needle electrode for radiofrequency tissue ablation: thermodynamic aspects of improved performance compared with conventional needle design. *Acad Radiol* 1996; **3**: 556–63.
15. Goldberg SN, Gazelle GS, Solbiati L, *et al.* Radiofrequency tissue ablation: increased lesion diameter with a perfusion electrode. *Acad Radiol* 1996; **3**: 636–44.
16. Kondo Y, Yoshida H, Tateishi R, *et al.* Percutaneous radiofrequency ablation of liver cancer in the hepatic dome using the intrapleural fluid infusion technique. *Br J Surg* 2008; **95**: 996–1004.
17. Dominique E, El Otmany A, Goharin A, *et al.* Intraductal cooling of the main bile ducts during intraoperative radiofrequency ablation. *J Surg Oncol* 2001; **76**: 297–300.
18. Raman SS, Aziz D, Chang X, *et al.* Minimizing central bile duct injury during radiofrequency ablation: use of intraductal chilled saline perfusion–initial observations from a study in pigs. *Radiology* 2004; **232**: 154–9.
19. Lam VW, Ng KK, Chok KS, *et al.* Safety and efficacy of radiofrequency ablation for periductal hepatocellular carcinoma with intraductal cooling of the central bile duct. *J Am Coll Surg* 2008; **207**: e1–5.
20. Ohnishi T, Yasuda I, Nishigaki Y, *et al.* Intraductal chilled saline perfusion to prevent bile duct injury during percutaneous radiofrequency ablation for hepatocellular carcinoma. *J Gastroenterol Hepatol* 2008; **23**(Part 2): e410–5.
21. Shiina S, Hata Y, Niwa Y, *et al.* Multiple-needle insertion method in percutaneous ethanol injection therapy for liver neoplasms. *Gastroenterol Jpn* 1991; **26**: 47–50.

Research Article

EASL EUROPEAN ASSOCIATION FOR THE STUDY OF THE LIVER | JOURNAL OF HEPATOLOGY

Altered composition of fatty acids exacerbates hepatotumorigenesis during activation of the phosphatidylinositol 3-kinase pathway

Yotaro Kudo[1], Yasuo Tanaka[1], Keisuke Tateishi[1,*], Keisuke Yamamoto[1], Shinzo Yamamoto[1], Dai Mohri[1], Yoshihiro Isomura[1], Motoko Seto[1], Hayato Nakagawa[1], Yoshinari Asaoka[1], Motohisa Tada[2], Miki Ohta[1], Hideaki Ijichi[1], Yoshihiro Hirata[1], Motoyuki Otsuka[1], Tsuneo Ikenoue[1], Shin Maeda[3], Shuichiro Shiina[1], Haruhiko Yoshida[1], Osamu Nakajima[4], Fumihiko Kanai[2], Masao Omata[5], Kazuhiko Koike[1]

[1]*Department of Gastroenterology, Graduate School of Medicine, The University of Tokyo, 7-3-1 Hongo, Bunkyo-ku, Tokyo 113-8655, Japan;* [2]*Department of Medicine and Clinical Oncology, Graduate School of Medicine, Chiba University, 1-8-1 Inohana, Chuo-ku, Chiba-shi, Chiba 260-8670, Japan;* [3]*Department of Gas troenterology, Yokohama City University, Graduate School of Medicine, 3-9 Fuku-ura, Kanazawa-ku, Yokohama 236-0004, Japan;* [4]*Research Laboratory for Molecular Genetics, Yamagata University, Yamagata 990-9585, Japan;* [5]*Yamanashi Prefectural Central Hospital, 1-1-1 Fujimi, Kofu-shi, Yamanashi 400-8506, Japan*

Background & Aims: Some clinical findings have suggested that systemic metabolic disorders accelerate *in vivo* tumor progression. Deregulation of the phosphatidylinositol 3-kinase (PI3K)/Akt pathway is implicated in both metabolic dysfunction and carcinogenesis in humans; however, it remains unknown whether the altered metabolic status caused by abnormal activation of the pathway is linked to the protumorigenic effect.

Methods: We established hepatocyte-specific *Pik3ca* transgenic (Tg) mice harboring N1068fs*4 mutation.

Results: The Tg mice exhibited hepatic steatosis and tumor development. PPARγ-dependent lipogenesis was accelerated in the Tg liver, and the abnormal profile of accumulated fatty acid (FA) composition was observed in the tumors of Tg livers. In addition, the Akt/mTOR pathway was highly activated in the tumors, and in turn, the expression of tumor suppressor genes including *Pten*, *Xpo4*, and *Dlc1* decreased. Interestingly, we found that the suppression of those genes and the enhanced *in vitro* colony formation were induced in the immortalized hepatocytes by the treatment with oleic acid (OA), which is one of the FAs that accumulated in tumors.

Conclusions: Our data suggest that the unusual FA accumulation has a possible role in promoting *in vivo* hepato-tumorigenesis under constitutive activation of the PI3K pathway. The *Pik3ca* Tg mice might help to elucidate molecular mechanisms by which metabolic dysfunction contributes to *in vivo* tumor progression.

Keywords: Hepatocellular carcinoma; Fatty acids; NAFLD; Tumor suppressor genes.

Received 3 October 2010; received in revised form 25 March 2011; accepted 27 March 2011; available online 19 May 2011

*Corresponding author. Tel.: +81 3 3815 5411x33070; fax: +81 3 3814 0021.

E-mail address: ktate-tky@umin.ac.jp (K. Tateishi).

Abbreviations: PI3K, phosphatidylinositol 3-kinase; Tg, transgenic; FA, fatty acid; OA, oleic acid; HCC, hepatocellular carcinoma; PTEN, phosphatase and tensin homolog deleted on chromosome 10; FBS, fetal bovine serum; Erk, extracellular signal-regulated kinase; WT, wild type; PA, palmitic acid; H&E, hematoxylin and eosin; NASH, non-alcoholic steatohepatitis.

Introduction

Accumulating clinical evidence suggests that systemic metabolic disorders including obesity and insulin resistance can affect or even promote *in vivo* tumor progression [1–4]. Some studies have outlined the impact of fat-enriched diets in the development of hepatocellular carcinoma (HCC) [5–7]. However, the mechanistic insights regarding metabolites or cellular signaling responsible for the development of HCC in altered metabolic states remain unknown.

The phosphatidylinositol 3-kinase (PI3K)/Akt signaling pathway is involved in various cellular processes including cell metabolism, growth, and survival [8,9]. The altered expression and mutation of PI3K/Akt-related signaling components have been detected in some human cancers [10]. In particular, the *PIK3CA* gene encoding p110α, which is a catalytic subunit of PI3K, has somatic mutations in some carcinomas [11]. Additionally, a mutation in its kinase domain has been reported in HCC and gastric cancer [12]. These findings indicate that deregulated PI3K activity plays certain roles in oncogenesis in humans [11,13]. PI3K signaling is antagonized by phosphatase and tensin homolog deleted on chromosome 10 (PTEN) phosphatase [14]. The expression of PTEN is decreased or absent in approximately half of HCC patients [15], and hepatocyte-specific *Pten* knockout

mice develop steatohepatitis and HCC [16]. These findings indicate that PTEN is a tumor suppressor in the liver [17]. Although recent reports have suggested unique functions of PTEN that are independent of the PI3K-Akt axis [18–20], it is unknown whether the phenotype in *Pten*-deficient mice is due to PI3K-dependent or PI3K-independent processes.

To address the pathological consequences caused by the abnormal activation of PI3K pathway *in vivo*, we generated liver-specific *Pik3ca* transgenic (Tg) mice. In this study, we proposed that abnormal fat composition, as observed in the *Pik3ca* Tg liver, is a mechanism by which metabolic deregulation is linked to *in vivo* tumor progression.

Materials and methods

Generation of Pik3ca Tg mice

The *Pik3ca* Tg mice were generated as described previously [21]. Briefly, Myc-tagged mouse *Pik3ca* cDNA (N1068fs*4) was cloned into the p2335A-1 vector (provided by Drs. Palmiter and Chisari) [22,23]. The microinjection was conducted by the Research Laboratory for Molecular Genetics, Yamagata University. Founder BDF1 mice (F0) were backcrossed with C57BL/6JJcl mice (CLEA Japan, Japan), and F5 mice were analyzed. The primers for genotyping were 5′-ATGGAACAGAAACTCATCTCT-3′ and 5′-GGGTGACACTTACGAAAAT-3′. All procedures involving animals were performed in accordance with protocols approved by the institutional committee for animal research at the University of Tokyo and complied with the Guide for the Care and Use of Laboratory Animals.

Cell cultures, viruses, and treatment with fatty acids

Lentiviral short hairpin RNA vectors were purchased from Open Biosystems (Huntsville, AL, USA). BNL-CL2 cells were infected with the virus according to the manufacturer's protocol and selected by puromycin. BNL-CL2 cells were incubated with either 50 μmol/L fatty acids or ethanol (mock) for 12 h in the absence of fetal bovine serum (FBS) in some experiments.

Antibodies and primers

The primers for quantitative RT-PCR are shown in Supplementary Table 1. Antibodies against phospho-Akt (Ser473 and Thr308), Akt, phospho-extracellular signal-regulated kinase (Erk) 1/2 (Thr202/Tyr204), Erk1/2, phospho-TSC2, phospho-S6K, TSC2, S6K, and SREBP1 were obtained from Cell Signaling Technology (Danvers, MA, USA). The anti-PTEN antibody was purchased from Neomarkers Inc. (Frement, CA, USA). The anti-TFIID antibody was purchased from Upstate Biotechnology Inc. (Lake Placid, NY, USA). For immunohistochemistry, the anti-phospho-Akt (Ser473) antibody and anti-Myc antibodies (Cell Signaling Technology) were used. The immunoblot data were quantified using Multi Gauge ver. 3.1 software (Fuji Film Corp., Tokyo, Japan).

Triacylglycerol content, serum alanine aminotransferase (ALT) levels, and FA composition

Triacylglycerols were extracted from the liver with chloroform–methanol (2:1, v/v), and the levels were determined by the GK-GPO method (Wako, Tokyo, Japan). Serum samples for ALT measurement were collected after a 16-h starvation (SRL, Tokyo, Japan). Fatty acids were extracted from frozen liver samples, and the composition was analyzed by gas chromatography (Kotobiken Medical Laboratories, Inc., Tokyo, Japan).

Glucose tolerance tests

Glucose was intraperitoneally injected into 8-week-old mice fasting for 16 h (1.5 mg of glucose/g body weight). Glucose concentration was measured using the FreeStyle FREEDOM Blood Glucose Monitoring System (Nipro, Tokyo, Japan) at 0, 15, 30, 60, 90, and 120 min after injection.

Oxidative stress evaluation

The measurement of hydrogen peroxide concentrations was performed by the Colorimetric Hydrogen Peroxide Kit (Assay Designs, Inc., Ann Arbor, MI, USA). Thiobarbituric acid reactive substances (TBARS) were measured by the TBARS Assay Kit (ZeptoMetrix, Buffalo, NY, USA).

Immunohistochemistry

Antigen retrieval on paraffin sections was performed by the acetylation method. Proteins were visualized using the standard 3,3′-diaminobenzidine protocol.

Soft agar assay

The lower layer of 0.5% agar in media was placed in a 35-mm dish. Cells (2.5×10^4) were suspended in the upper layer of 0.3% agar. Colonies (>25 μm in diameter) were counted after 14 days. Oleic acid (OA) (50 μmol/L) or ethanol was added to the upper layer in some experiments.

Statistics

All results are indicated as means ± SE. Statistics were performed by Student's *t*-test or ANOVA followed by Fisher's PLSD host-hoc test. *p*-Values <0.05 were considered statistically significant.

Results

Generation of hepatocyte-specific Pik3ca Tg mice

We established 2 independent lines of hepatocyte-specific Tg mice (*Pik3ca* Tg mice) harboring an "N1068fs*4" mutation in the kinase domain [12]. Myc-tagged mutant *Pik3ca* was designed to be expressed under the albumin promoter (Supplementary Fig. 1), and the liver-specific expression of the transgene was confirmed as shown in Fig. 1A. To assess the *in vivo* effect of the *Pik3ca* N1068fs*4 transgene, we analyzed the activity of molecules downstream of PIK3CA including Akt, TSC2, and S6K via immunoblotting. The phosphorylation of Akt, TSC2, and S6K was clearly increased both in the two lines of Tg livers, but not in the wild-type (WT) livers (Fig. 1B).

Constitutive activation of Pik3ca leads to fat accumulation in the liver

Both lines of *Pik3ca* Tg mice survived, and no difference in total body weight was observed between *Pik3ca* Tg and WT mice at 4 or 24 weeks of age (data not shown). The *Pik3ca* Tg2 mice exhibited better glucose tolerance than WT mice at 8 weeks (Supplementary Fig. 2). The ratio of liver weight to body weight was significantly increased in the *Pik3ca* Tg mice compared to that of WT mice (Fig. 2A). The livers of 4 week-old *Pik3ca* Tg mice appeared slightly enlarged and light-colored, and they exhibited obvious fatty changes by 24 weeks (Fig. 2B). The Tg livers contained a greater volume of triacylglycerol than WT (Fig. 2C). The results of Western blotting revealed that Tg2 mice exhibited a relatively low activation of Akt and S6K as compared to Tg1 (Fig. 1B); however, hepatic triacylglycerol levels were clearly increased in the two lines Tg mice (Fig. 2C). Indeed, even Tg2 mice demonstrated an obvious fatty change in their livers by 24 weeks (Fig. 2B and D). These findings indicated that the constitutive expression of the *Pik3ca* N1068fs*4 transgene has a potential to establish *in vivo* hepatic steatosis. In addition, we found

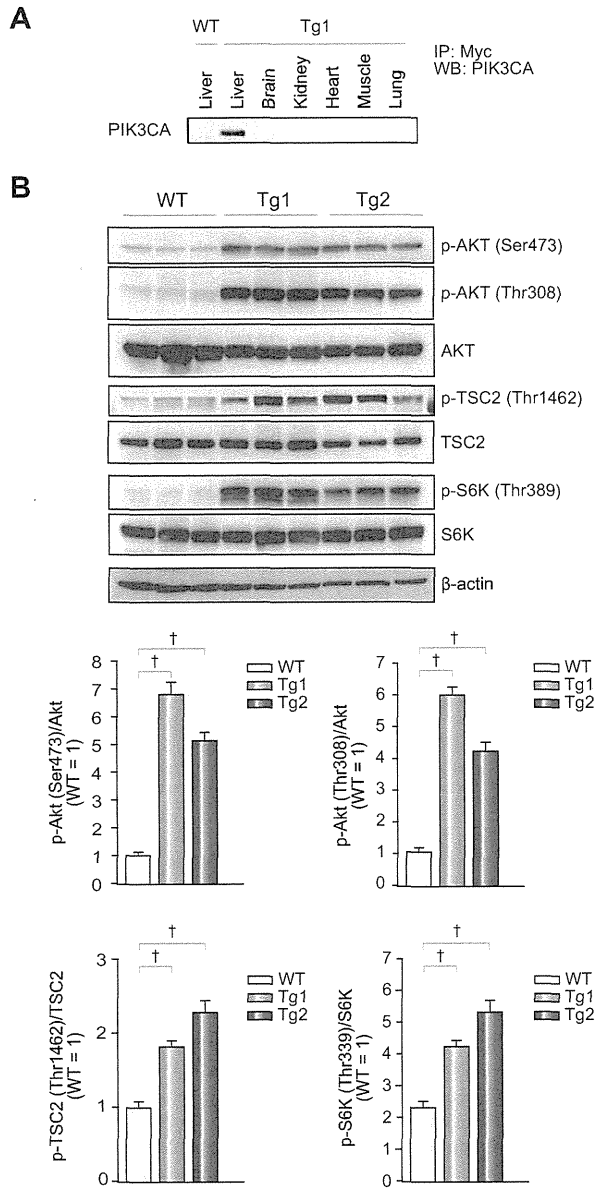

Fig. 1. Establishment of *Pik3ca* Tg mice. (A) Liver-specific expression of the mutant PIK3CA (N1068fs*4). (B) Immunoblots and quantification of the ratios of phosphorylated-Akt, TSC2, and S6K levels to total protein levels (†$p < 0.05$, ANOVA; post hoc test with WT).

that ALT levels in the *Pik3ca* Tg mice were higher than those of WT mice (Fig. 2E), suggesting the coexistence of liver damage. Next, we examined how the *Pik3ca* Tg liver induced unusual lipid accumulation. Because lipogenesis is mainly mediated by two major transcription factors, PPARγ and SREBP1C [24,25], we measured their expression levels and their target genes in Tg2 mice livers and observed the upregulation of PPARγ and its target aP2 but not of SREBP1C or its target FASN (Fig. 2F). Given the previous finding that activated PI3K signaling can induce steatosis through PPARγ [26], we speculated that PPARγ-dependent lipogenesis is a process responsible for hepatic steatosis in Tg mice. This was supported by the finding that the nuclear accumulation of the active form of SREBP1c protein was not increased by *Pik3ca* (N1068fs*4) expression (Supplementary Fig. 3). To emphasize this notion, we investigated whether the *in vitro* overexpression of *Pik3ca* (N1068fs*4) induced lipid accumulation and the activation of PPARγ-dependent transcription. The *in vitro* overexpression of *Pik3ca* (N1068fs*4) increased the concentration of triacylglycerol in BNL-CL2 cells, immortalized normal hepatocytes derived from a BALB/c mouse [27] (Fig. 2G), and upregulated *aP2* expression (Fig. 2H). These data indicated that the overexpression of *Pik3ca* (N1068fs*4) directly contributes to the enhanced lipogenesis, at least via activating PPARγ-dependent transcription. Given the important role of mTOR in lipogenesis through PPARγ, there is a possibility that the activation of mTOR signaling (Fig. 1B) contributes to deregulated lipogenesis through PPARγ signaling in the *Pik3ca* Tg liver [26].

Tumor formation without inflammation in the Pik3ca Tg mice

Regardless of the marked fatty changes and suggested liver damage, *Pik3ca* Tg livers did not exhibit cellular infiltration or fibrotic change even at 52 weeks of age (Fig. 3A and B), which means the expression of the *Pik3ca* transgene is not sufficient for progression to steatohepatitis in the mouse liver. We found that the inflammatory cytokine IL-1α and Fas ligand were highly expressed in the *Pik3ca* Tg liver than WT (Supplementary Fig. 4). Given the previous findings that these factors can be responsible for liver damage [28,29], the abnormal upregulation of IL-1α and Fas ligand in Tg livers may explain a part of the mechanisms of liver damage, whereas the entire molecular process inducing them remains unknown. Notably, macroscopic hepatic tumors developed in 94% of Tg1 mice (30/32) and 100% of Tg2 mice (11/11) at 52 weeks of age (Fig. 3C, left). Most of the tumors were hepatocellular adenomas containing abundant lipid droplets (Fig. 3C, right). Some tumors had rough surfaces and irregular shapes with necrosis and hemorrhaging (Fig. 3D, left) and microscopically demonstrated characteristics of HCC such as enlarged and hyperchromatic nuclei and trabecular patterns (Fig. 3D, right). HCC tissues did not always exhibit lipid accumulation as shown in Fig. 3D. As the *Pik3ca* Tg mice aged, hepatic tumors became increased in number and size, whereas no WT littermates developed any tumors (Fig. 3E). These data clearly indicate that the *in vivo* constitutive expression of *Pik3ca* (N1068fs*4) leads to hepatic tumor development. To assess the functional activity of PIK3CA (N1068fs*4) for tumorigenesis, we examined the *in vitro* transforming ability using BNL-CL2 cells. Remarkably, *Pik3ca* (N1068fs*4) expression did not stimulate colony formation of BNL-CL2 cells (Supplementary Fig. 5). In addition, we analyzed the phosphorylation level of Akt by the *in vitro* overexpression of *Pik3ca* genes including wild type, H1047R, or N1068fs*4 in 293T cells. The overexpression of *Pik3ca* (H1047R) possessing *in vitro* transforming capacity [13] resulted in strong phosphorylation of Akt, as previously reported (Supplementary Fig. 6) [30]. Conversely, the overexpression of *Pik3ca* (wild type) without any transforming capacity [13] resulted in lower phosphorylation of Akt. The mutant PIK3CA (N1068fs*4) induced phosphorylation of Akt, but the level was comparable to that of wild type, and less than that of H1047R (Supplementary Fig. 6). These findings suggested that *Pik3ca* (N1068fs*4), as compared to H1047R, has less capacity for activating Akt and little